Tectonophysics 489 (2010) 189–209

Contents lists available at ScienceDirect

Tectonophysics

journal homepage: www.elsevier.com/locate/tecto

New constraints to the onset of the India–Asia collision: Paleomagnetic reconnaissance on the Linzizong Group in the Lhasa Block, China

Junshan Chen, Baochun Huang *, Lisha Sun

Paleomagnetism and Geochronology Laboratory of the State Key Laboratory of Lithospheric Evolution, Institute of Geology and Geophysics of the Chinese Academy of Sciences, Beijing 100029, China

ARTICLE INFO

Article history:
Received 31 July 2009
Received in revised form 16 April 2010
Accepted 19 April 2010
Available online 25 April 2010

Keywords:
Linzizong Group
Paleomagnetism
Lhasa Block
Paleogeographic position
India–Asia collision

ABSTRACT

To better understand the onset of the India–Asia collision, a paleomagnetic study has been conducted on Paleogene volcanic rocks and sediments of the Linzizong Group (~64–44 Ma) from the Linzhou and Namling basins of the Lhasa Block at the southern margin of the Asian continent. Following detailed rock magnetic investigations and progressive thermal or hybrid thermal and alternating field demagnetization, stable characteristic remanent magnetizations (ChRMs) were successfully defined from the Dianzhong (~64–60 Ma), Nianbo and Pana (~60–44 Ma) formations. These ChRMs are of dual polarity, and pass a fold test with some of them in volcanic rocks carried by oxidation-induced hematite; we thus interpret them as primary remanences. Paleomagnetic results from the bulk of the collection imply that the southern leading edge of Asia, i.e. the Lhasa Block, remained essentially stationary in low latitudes at ~10°N without paleomagnetically-detectable tectonic rotation and latitudinal variation during the formation of the Linzizong Group. Consequently, a large-scale post-collisional northward convergence in the Tibetan plateau and central Asia is very likely to have occurred after formation of the Linzizong Group, and the definitive paleoposition of the Lhasa Block during the period embracing the interval between ~64 and 44 Ma provides further constraints on the latitudinal position of the initial contact between India and Asia. This evidence rules out the model for a younger (~35 Ma) India–Asia collision and implies that the initial India–Asia collision occurred between ~65 and 50 Ma. Given that Greater India comprised the present Indian continent together with a ~950 km extension beyond its northern margin prior to the rifting of Gondwana in the Middle Jurassic, we conclude that the initial India–Asia collision most probably occurred between ~55 and 60 Ma.

1. Introduction

The India–Asia collision was responsible for creating the Himalaya–Tibetan Orogen (Fig. 1) which is a focus of much present day solid Earth research and is considered to be one of Earth's most fascinating Phanerozoic tectonic episodes (e.g. Dewey et al., 1989; Matte et al., 1997; Yin and Harrison, 2000). The progressive evolution of this orogen has led to formation of the Himalaya and uplift of the Tibetan plateau. It has also been responsible for reorganizing the drainage system in SE Asia leading in turn, to the formation of the Asian monsoon and changes in regional environments; it has probably also had a significant effect on global climate (Raymo and Ruddiman, 1992; Molnar et al., 1993; Brookfield, 1998; Clark et al., 2004). Whilst the timing of collision between India and Asia is obviously not the only key boundary condition for modeling the evolution of the Himalaya–Tibetan orogenic system (Aitchison et al., 2007), it is an important starting point for discussion of the formation of the orogenic system and accompanying plateau uplift. The question of this timing has been the subject of much dispute during the past decade. Whilst noting that the geoscience community generally tends to view the time interval ~55–50 Ma as the onset of the India–Asia collision (e.g. Patriat and Achache, 1984; Klootwijk et al, 1992), other studies have more recently proposed that initial contact between India and Asia occurred at times ranging from the late Cretaceous (~70 Ma) to the early Oligocene (~34 Ma) (e.g. Aitchison et al., 2000, 2007; Aitchison and Ali, 2001; Ding et al., 2003; Mo et al., 2003, 2008; Ali and Aitchison, 2008).

Studies interpreting the Cretaceous/Paleogene (K/Pg) boundary at ~65 Ma as the onset of the India–Asia collision (Ding et al., 2003, 2005; Mo et al., 2003, 2008; Zhu et al., 2004) have followed from analysis of tectonic deformation on both sides of the Indus–Yarlung Zangbo Suture Zone (IYSZ). This view is in accord with biological connectivity observed between the Indian and Asian continents (Jaeger et al., 1989; Prasad and Rage, 1991; Rage et al., 1995; Briggs, 2003) and is also compatible with the conclusion derived from comprehensive multidisciplinary information

* Corresponding author. Institute of Geology and Geophysics, Chinese Academy of Sciences, Bei Tuchen Xilu, Chaoyang District, Beijing 100029, China. Tel.: +86 10 82998412; fax: +86 10 62010846.
E-mail addresses: bchuang@mail.iggcas.ac.cn, bchliv05@yahoo.com (B. Huang).

0040-1951/$ – see front matter © 2010 Elsevier B.V. All rights reserved.
doi:10.1016/j.tecto.2010.04.024

from the plateau by Yin and Harrison (2000). In contrast, some other studies have proposed a revised model describing the Late Cretaceous–Paleogene passage of India towards the Lhasa Block of Asia in terms of a collision between India and an island arc system during the early Paleogene at ~57–55 Ma followed by collision between the Indian plate and Lhasa Block at the Eocene/Oligocene boundary at ~34 Ma (Aitchison et al., 2000, 2007; Aitchison and Ali, 2001; Ali and Aitchison, 2008). The former continent–arc system collision might then be responsible for previously-observed collisional evidence around the *K*/*Pg* boundary in the Indian and Asian continents, whereas the latter collision may define the real time of initial collision between India and Asia. Compared with the traditional model, this revised India–Asia collision model requires that the southernmost margin of the Lhasa Block retained its approximate present position at ~30°N (Fig. 11–12 of Ali and Aitchison, 2008) rather than residing at low latitudes of ~10°N in the Northern Hemisphere (e.g. Patriat and Achache, 1984; Klootwijk et al., 1992; Tong et al., 2008) prior to the initial contact between India and Asia.

Since paleomagnetism is the only effective method for quantifying paleogeography and constraining kinematic processes of plate movement, a large number of paleomagnetic studies have been carried out to determining the time of India–Asia collision. From analyses during the mid-1970's of magnetic lineations in the Indian Ocean, Molnar and Tapponnier (1975) found that the rate of motion of the Indian plate relative to Eurasia had decreased dramatically in the Cenozoic. They interpreted the timing of a velocity reduction from 10–16 to 5 cm/yr (~40 Ma) in terms of the onset of the India and Asia collision. From re-analysis of the data, Patriat and Achache (1984) inferred that initial collision between India and Asia occurred around ~50 Ma when the velocity declined from 15–20 to <10 cm/yr. From paleomagnetic study of sedimentary rocks at the Ninetyeast ridge of the Indian Ocean Klootwijk et al. (1992) identified a distinct reduction in northward drift velocity of the Indian plate from 18–19.5 to 4.5 cm/yr at ~55 Ma and speculated that initial contact between India and Asia actually occurred prior to this. However, whether these dramatic changes in the rate of plate motion were caused by the collision of another plate or by changes of spreading rate of the Indian Ocean Ridge are still debated. Assuming that the ubiquitous remagnetization components present in late Paleozoic to mid-Cretaceous rocks on both sides of the IYSZ were caused by the India–Asia collision, Klootwijk et al. (1994) inferred that the onset of the India–Asia collision should have occurred at or before ~65 Ma. They based this conclusion on the comparable paleogeographic locations of the suture zone and the northwestern margin of Greater India as calculated from remagnetization components compared with the apparent polar wander (APW) path of India (Klootwijk and Peirce, 1979). Nevertheless when the Greater India model of Klootwijk et al. (1992, 1994) is examined in the context of recently-updated APW paths for India (Acton, 1999; Besse and Courtillot, 2002; Schettino and Scotese, 2005; Torsvik et al., 2008) the northwestern margin of Greater India is not found to drift across the equator and reach low latitudes in the Northern Hemisphere near the *K*/*Pg* boundary.

A possibility to address this problem is provided by a suite of volcanic rocks and intercalated sedimentary layers, assigned to the Linzizong Group, widely distributed in the southern part of the Lhasa Block (Fig. 1). These volcanic rocks are of syn- or post-collisional character (Mo et al., 2003, 2006; Dong et al., 2005), and are likely to record key information on the India–Asia collision. Paleomagnetic study of the Linzizong volcanic rocks began at the end of the 1970's by a Sino–French scientific expedition (Zhu et al., 1981; Zhu and Teng, 1984; Westphal et al., 1984; Zhou et al., 1990; Achache et al., 1991). However, owing to insufficient understanding of the chronological framework of the group and technical limitations to the paleomagnetic measurement and analysis, these preliminary paleomagnetic results were unable to accurately define paleogeographic location and possible motion of the Lhasa Block during formation of the Linzizong Group at ~64–44 Ma. Renewed investigation employing modern methods and a wider distributed sample is therefore required to constrain the onset of India–Asia collision.

In the investigation reported in this paper, we have performed a paleomagnetic study on Linzizong volcanic rocks and intercalated sediments collected from both the Linzhou and Namling basins of the Lhasa Block (Figs. 1 and 2) and we interpret the data in the context of a newly redefined chronological framework for the group (Zhou et al., 2001, 2004; Dong et al., 2002, 2005; Mo et al., 2003). We thereby aim to provide accurate paleomagnetic constraints on the paleogeography of the southern leading edge of the Asian continent (Lhasa Block) during Linzizong Group times. This enables us to discuss when, and where, Greater India made contact with the Asian continent.

2. Regional geological structure and paleomagnetic sampling

As shown in Fig. 1, the Himalaya–Tibetan plateau is located between India and central Asia, and consists from north to south of the Qaidam, Songpan–Ganze, Qiangtang, Lhasa, and Himalayan blocks. In general terms the plateau is thought to be formed by a series of drift, subduction, collision and intracontinental orogenic process within the above-mentioned micro-continental blocks (e.g. Xu et al., 2006). These blocks are separated by several active tectonic zones, some of which comprise former sutures, including the Ayimaqin–Kunlun–Muztagh Suture (AKMS), Jinsha River Suture (JS), Bangong–Nujiang Suture (BNS), Indus–Yarlung Zangbo Suture (IYS), Main Central Thrust (MCT), and Main Boundary Thrust (MBT) from north to south (Fig. 1). The IYSZ is regarded as the extinction zone of the Neo-Tethys Ocean and the final collision zone between the Indian and Asian continents (e.g. Chang et al., 1986; Yin and Harrison, 2000). In the north of the IYSZ, there is a large number of Gangdise back-arc basins developed at the southern part of the Lhasa Block with the Linzhou Basin to the north of the city of Lhasa and the Namling Basin to the north of the city of Shigatse being the examples (Lu et al., 2000; Zhang et al., 2007). In the Linzhou Basin, Linzizong volcanic rocks and intercalated sediments are exposed along the southern part of the Lhasa Block (Wang et al., 1988; Song, 1999; Mo et al., 2003; Huang et al., 2004, 2005b; Wu et al., 2005; Hu et al., 2007) where they both have a wide distribution (Figs. 1 and 2) and a long temporal duration between ~64 and 44 Ma (Zhou et al., 2001, 2004).

The Linzizong Group was originally defined during the 1950's as a volcanic succession without intercalated sedimentary layers or unconformities. However during the 1990's, geological surveys found a number of unconformities and lithologic differences within the group and it has subsequently been divided into three formations comprising the Dianzhong, Nianbo, and Pana formations in ascending order (TRGST, 1990; Liu, 1993). Dong et al. (2002, 2005) embarked on a geological mapping study in the Linzhou Basin (Figs. 1 and 2a) and further classified the Linzizong Group into three formations and eight sections on the basis of Ar–Ar geochronological measurements (Fig. 2c–d and Zhou et al., 2001, 2004). The findings of these new studies provide the basis for our paleomagnetic reconnaissance of this group.

In the Linzhou Basin (Fig. 1), the Paleogene Linzizong Group unconformably overlies a suite of red sediments comprising the Late Cretaceous Shexing Formation and is unconformably overlain by a succession of Quaternary terrigenous sediments. All three members, the Dianzhong, Nianbo, and Pana formations, are well-developed with clear boundaries between them (Fig. 2c and TRGST, 1990, 1991; Ke, 1990; Dong et al., 2005; Ji et al., 2006). Following the 1:50,000 geological mapping of volcanic rocks in the basin (Dong et al., 2005), a total of 302 oriented drill-core samples (34 sites) have been collected from both volcanic rocks and intercalated sedimentary rocks. The selected sampling sections are mainly distributed in the vicinity of the Dianzhong and Pana villages, and the Nagagunba and Xiagunba temples (Fig. 2a); the bedding attitudes are generally N-NNE-dipping with fairly low tilts of ~20–40°. For the Dianzhong Formation, the

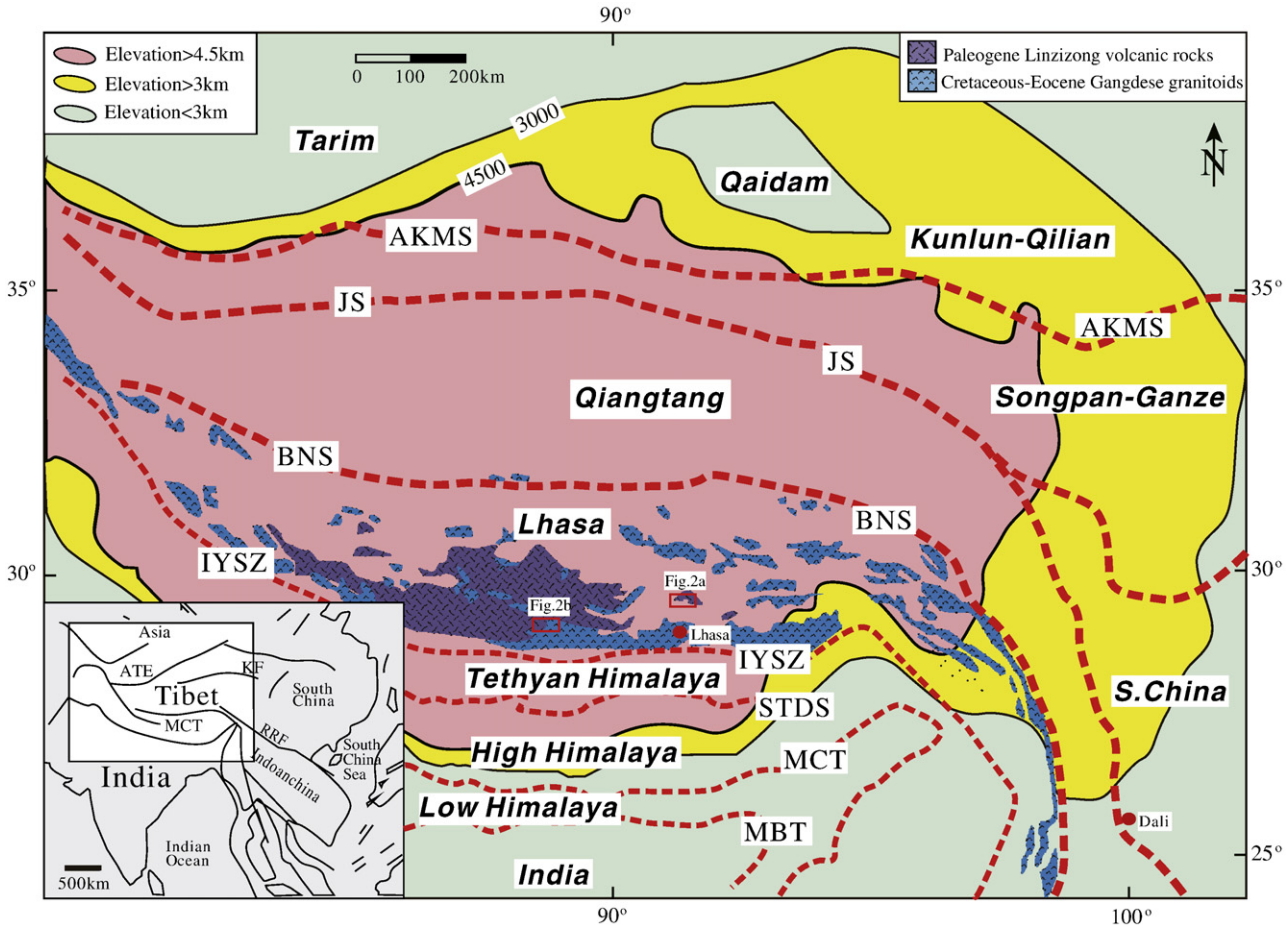

Fig. 1. Schematic geological map showing the tectonic framework of the Himalaya–Tibetan plateau and surrounding areas after Chung et al. (2005). The distributions of the Cenozoic Linzizong Group and Cretaceous–Eocene Gangdise granitoids in the Lhasa Block are also shown in this figure. Elevations of the plateau are after Fielding et al. (1994). Inset shows tectonic framework in western China and surroundings. Abbreviations are: AKMS, Ayimaqin–Kunlun–Muztagh Suture; BNS, Bangong–Nujiang Suture; IYSZ, Indus–Yarlung Zangbo Suture Zone; JS, Jinsha Suture; MBT, Main Boundary Thrust; MCT, Main Central Thrust; STDS, South Tibet Detachment System.

sampled sections are situated in Kaibu, Nagagunba–Xiagunba, and Chongga areas (Fig. 2a) and a total of 133 drill-core samples in purple and pink andesites and tuffs were collected from 16 sites. For the Nianbo Formation, sampling sections are distributed in the vicinity of Xiagunba and Renjigang villages (Fig. 2a) and comprise 58 drill-cores from 6 sites in purple sandstones from the lower part in Xiagunba, and 38 core samples from 4 sites in argillaceous limestones from the middle part of the formation in the village of Renjigang. The 68 drill-core samples (8 sites) from the Pana Formation were all collected from the vicinity of the village of Gulu (Fig. 2a) and all samples comprise andesitic or rhyolitic volcanic rocks. Fig. 2c gives a stratigraphic summary of all the sampling sites in the basin, with respect to the geochronology of Zhou et al. (2004).

The stratigraphic succession developed in the Namling Basin (Fig. 1) consists of, in ascending order, the Chumulong and Takena formations (Early Cretaceous), the Shexing Formation (Late Cretaceous), the Linzizong Group and the Rigongla Formation (Paleogene) and the Magnxiang Formation (Neogene). The Linzizong Group is also divisible into the Dianzhong, Nianbo, and Pana formations (Fig. 2d and TRGST, 1990; GSTAR, 2002) although both geological and geochronologic studies of the Linzizong Group in this basin lag far behind investigation of the Linzhou Basin. Consequently, only the Dianzhong and Nianbo formations, which are both easily identified in the field, were selected for sampling. As shown in Fig. 2b, all sites were located along a country road linking the Tangba, Laya, and Jiare villages. In total, 66 drill-core samples at 7 sites and 110 drill-core samples at 11 sites were collected from the Dianzhong and Nianbo formations, respectively. For the Dianzhong Formation, which is in contact with the underlying Shexing Formation by unconformity, the collected samples comprise purple andesites and brownish-red tuffaceous dacites; samples from the Nianbo Formation consist entirely of intercalated red sediments.

All the core samples were collected with a portable petrol-powered drill and oriented by sun compass. Some sites were oriented by both sun and magnetic compasses in order to evaluate any differences between local declinations and the present International Geomagnetic Reference Field in the sampling area.

3. Rock magnetic results

Following sample preparation, one pilot sample from each site was subject to rock magnetic experiments comprising acquisition of isothermal remanent magnetization (IRM), back-field demagnetization of saturation IRM (SIRM), hysteresis loop, and thermomagnetic analysis in order to better understand magnetic mineralogy. The acquisition of IRM, back-field demagnetization of SIRM, and hysteresis loops were performed using either a variable field translation balance (VFTB) with a maximum field generated by direct current (DC) of 10 A (approximately 2.79 A/m) or by MicroMag 2900 and 3900 alternating gradient magnetometers. Magnetization versus temperature curves (J–T curves) were measured by the VFTB in an equivalent DC field of ~1.4 A/m (5 A); whilst magnetic susceptibility versus temperature curves (k–T curves) were conducted using a KLY-3 kappa bridge coupled with a CS-3 apparatus. Rock magnetic measurements and

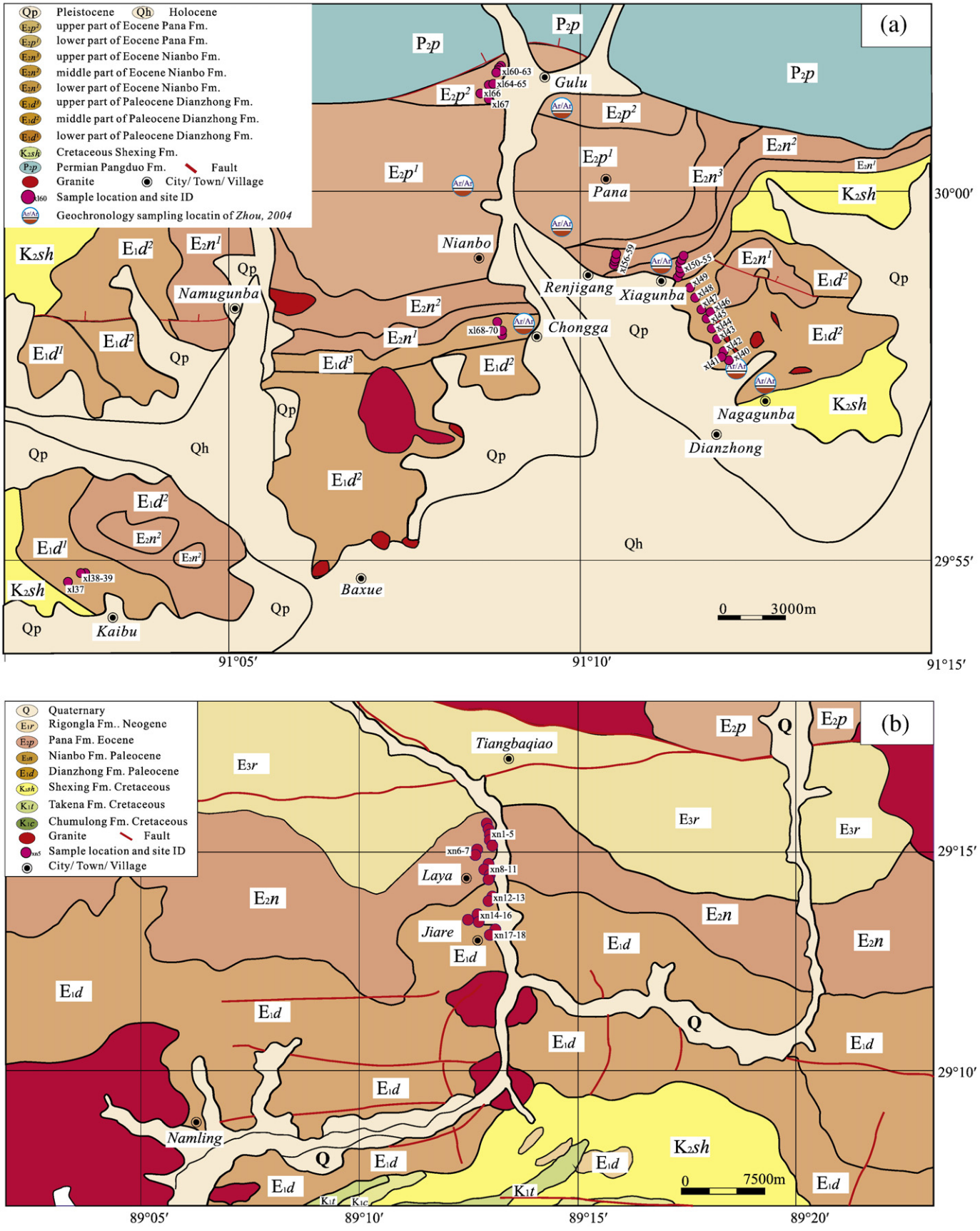

Fig. 2. (a–b) Simplified regional geological maps of the Linzhou and Namling basins showing distributions of paleomagnetic sampling locations (red solid circles), modified from Dong et al. (2005) and the regional geological map of Shigatse (GSTAR, 2002), respectively. Circles with "Ar" represent geochronological sampling locations (Zhou et al., 2004); (c–d) Post-late Cretaceous stratigraphy for the Linzhou and Namling basins, respectively. Paleomagnetic sampling and geochronological sampling (Zhou et al., 2004) layers are approximately indicated by "P" and "Ar" in the plots.

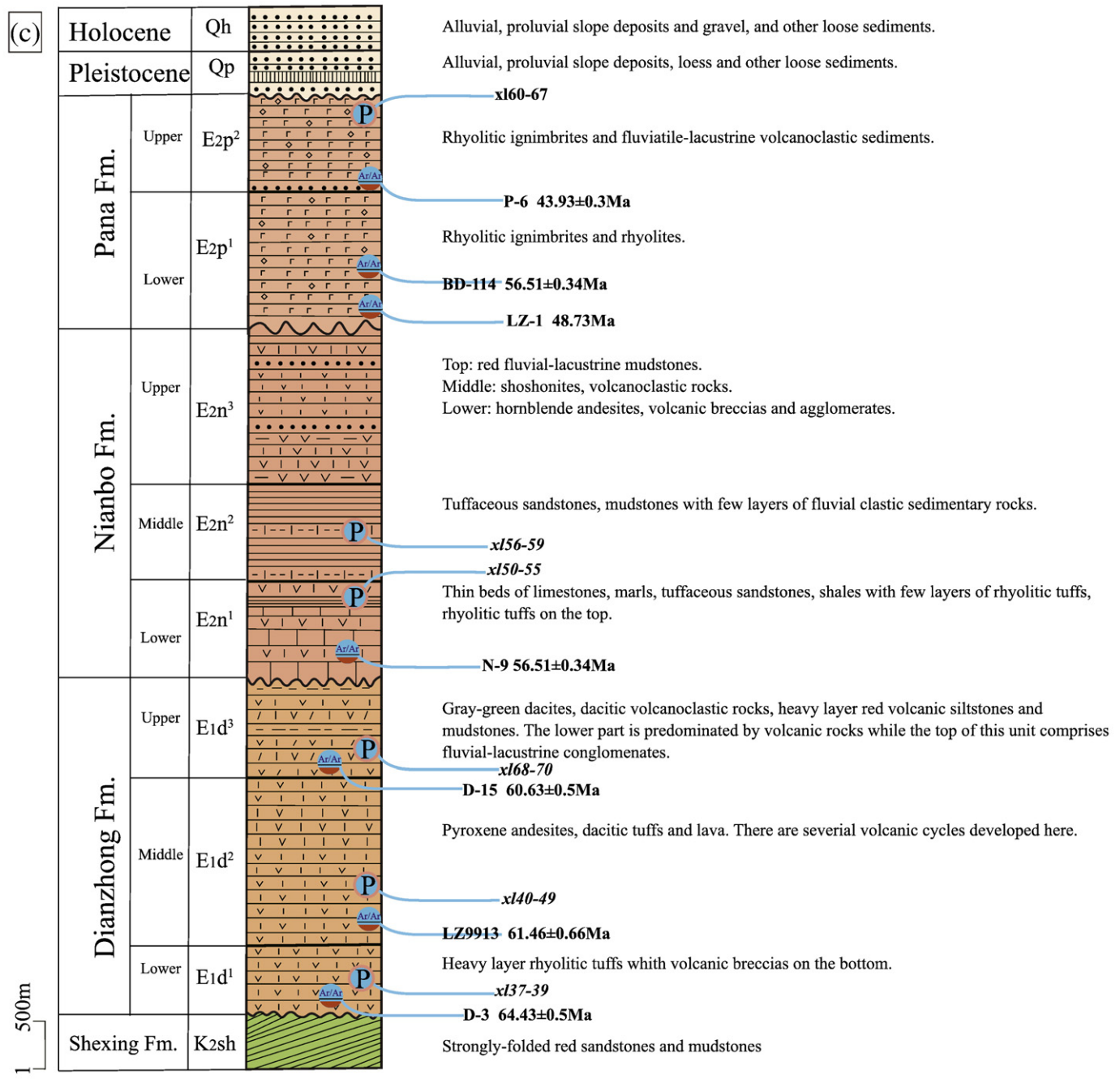

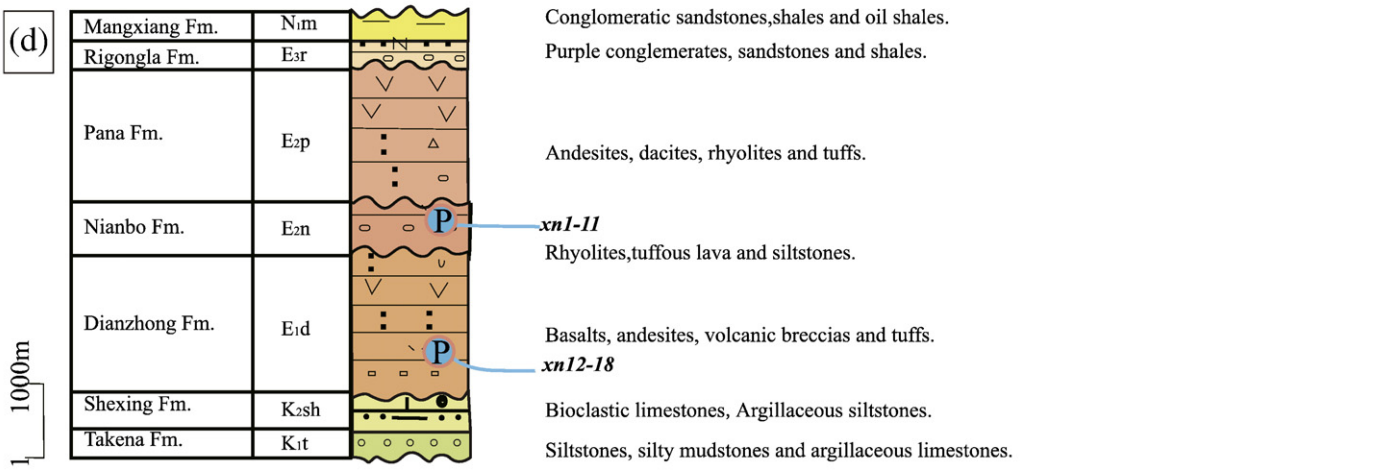

Fig. 2 (*continued*).

subsequent paleomagnetic experiments were performed in the Paleomagnetism and Geochronology Laboratory (PGL) of the Institute of Geology and Geophysics, Chinese Academy of Sciences.

As shown in Fig. 3, all the measured samples can be classified into three categories according to rock magnetic properties. Firstly, gray tuffs samples (sites xn10, xn11 and xl56) and limestone samples (site xl58) collected from the Nianbo Formation in the two basins are characterized by approximately reversible *J–T* or *k–T* curves with unblocking temperatures of ~580 °C (Fig. 3g). Together with typical low-coercivity implied by IRM acquisition and back-field demagnetization of SIRM curves (Fig. 3a), magnetite is identified as the main magnetic mineral. The ratios, $Mrs/Ms = 0.22$ and $Bcr/Bc = 1.95$, computed from the measurement of hysteresis loop (Fig. 3d) further indicate a pseudo-single-domain (PSD) state for the magnetite grains (Day et al., 1977).

Secondly, purple-red fine-grained sandstones (sites xl50-51, xl54-55), argillaceous limestones (xl57, 59), pink andesites, rhyolitic andesites and tuffs (xl37-39, xl52-53, xl60-63, xl66-69), and tuffaceous dacites (xn15-16, xn18) also exhibit approximately reversible *J–T* or *k–T* curves during the heating–cooling run, indicative of insignificant changes in the mineral phases during the heating. A distinctive drop of magnetization or magnetic susceptibility around 580 °C and 670–690 °C (Fig. 3h), a rapid increase/drop trend of the IRM during the initial stage of IRM acquisition/back-field demagnetization and subsequent increase of IRM in a maximum pulse magnetic field of 2.0 T (Fig. 3b) together with the wasp-waisted hysteresis loop (Fig. 3e) all collectively suggest that (titano)magnetite and (deuteric oxidation-induced) hematite are the main magnetic minerals. Purple-red sandstone or marlaceous sandstone samples in sites xn3 and xn5-8 collected from the Namling Basin showed roughly similar rock magnetic behaviors to the samples of this category. However, magnetite might be absent or appear as a subordinate magnetic mineral because of a much more potbelly-shaped hysteresis loop and insignificant increase of IRM during the initial stage of the IRM acquisition.

The third category comprises pink andesites (xl40-49), rhyolitic andesites (xl64-65), tuffs (xn1 and xn2), sandstones (xn4 and xn9) and a few tuffaceous dacites (xn17). Samples in this category are characterized by either irreversible *J–T* curves with significant loss of magnetization after the heating (Fig. 3i) or by irreversible *k–T* curves with distinguishable drop of magnetic susceptibility during the heating up to ~460 °C (Fig. 3j). Significant decrease of both magnetization and magnetic susceptibility around ~300–400 °C during the heating cycle (Fig. 3i–j) implies that an inversion or oxidation of maghemite to hematite may have occurred during the heating in air (Dunlop, 1995). Noting that IRM acquisition, back-field demagnetization (Fig. 3c) and the hysteresis loop (Fig. 3f) each suggest the predominance of low-coercivity ferromagnets in the sample; the slight but significant decrease of magnetization above ~650 °C (Fig. 3i) indicating a presence of hematite suggests that the hematite observed in the heating–cooling run in air results from inversion or oxidation of maghemite. Thus, the low-coercivity of remanence and two significant decreases of magnetization and magnetic susceptibility around ~300–400 °C and ~550–600 °C during the heating (Fig. 3i–j) indicate that various phases of (titano)magnetite plus maghemite are the main ferromagnets in these samples.

4. Paleomagnetic results

Following evaluation of rock magnetic behaviors resolved from pilot samples, about 8 specimens per site were subjected to either progressive thermal or AF demagnetization. In general, progressive thermal demagnetization was applied to specimens when the pilot samples exhibited approximately reversible thermomagnetic behavior, whereas progressive AF demagnetization or an integrated approach comprising thermal demagnetization to 250 °C followed by AF demagnetization up to 89 mT was applied to sites where pilot samples showed irreversible thermomagnetic curves. Thermal demagnetization was carried out in a TD-48 thermal demagnetizer with residual magnetic field minimized to <10 nT inside the cooling chamber. Demagnetization intervals were 50 °C at lower temperatures, and subsequently reduced to increments as small as 10 °C at higher temperatures as maximum unblocking temperatures of the remanence carriers were approached. Progressive AF demagnetization was conducted using an AF demagnetizer 2G600 coupled to a 2G-755 cryogenic magnetometer in steps of 5 or 10 mT. All remanence measurements were performed on a 2G-755 cryogenic magnetometer. Both demagnetizer and magnetometer are installed in a magnetically shielded space with the field inside minimized to <300 nT. Demagnetization results were plotted onto orthogonal diagrams (Zijderveld, 1967) and stereographic projections with the former used to resolve components by principle component analysis (Kirschvink, 1980); mean directions were calculated using standard Fisher statistics (Fisher, 1953) or the method of combined remagnetization circles and direction observations (McFadden and McElhinny, 1988).

4.1. Linzhou Basin

4.1.1. Dianzhong Formation

For the lower part of this formation, 27 specimens in 3 sites (xl37-39) were collected from the vicinity of the village of Kaibu (Fig. 2a). Progressive thermal demagnetization mostly showed the presence of two magnetic components following the removal of a viscous component in the initial stage of demagnetization up to ~100/150 °C (Fig. 4a). The low or intermediate temperature component (assigned as LTC hereafter) was often removed completely by temperatures of ~450–500 °C; a high temperature component (HTC) could subsequently be isolated at temperatures between ~500/530 °C and 690 °C with the majority unlocked by temperatures >630 °C (Fig. 4a) and the minority by temperatures around 580 °C. However, either the LTC or HTC show within-site dispersion of the directions before or after tilt adjustment (Figs. 6a–b and 7a–b). This is probably due to the presence of large lithic fragments in the specimens and all the samples from this collection were discarded from further analysis.

For the upper part of this formation, 25 specimens in 3 sites (xl68-70) were drilled from the village of Chongga (Fig. 2a), and 12 out of 15 demagnetized specimens yielded stable HTC after the removal of viscous overprinting and LTC by temperatures of 400–450 °C with unblocking temperatures around 580 °C in site xl70 (Fig. 4 g) or >650 °C in sites xl68-69. We have combined the magnetic components isolated from this unit into the collection from the middle part of this formation.

For the middle part of the formation, 10 sites (xl40-49) were drilled from a profile between the Nagagunba and Xiagunba temples (Fig. 2a). Progressive thermal or AF demagnetizations for most specimens show the presence of two magnetic components following removal of a viscous component in the initial stage of demagnetization (Fig. 4b–f). The LTC was mostly removed by ~250–300 °C or 5–10 mT by hybrid thermal and AF demagnetization (Fig. 4b–e). Together with those components isolated from specimens in the upper part of the formation, the LTC directions show a scattered distribution without meaningful group-mean directions either before or after tilt correction (Fig. 6a–b) indicating that this LTC might result mostly from viscous overprinting. The HTC could be completely removed by temperatures of 650–690 °C (Fig. 4c–d) or AF fields of 40–80 mT after an initial thermal treatment up to ~250 °C (Fig. 4b, e) suggesting that it is carried by either magnetite or hematite. As shown in Fig. 4d, this component may also be carried by both magnetite and hematite in a specimen because directions computed from the AF demagnetization interval and subsequently thermal demagnetization up to 690 °C are statistically identical. Nevertheless some specimens yielded a great circle distribution of demagnetization trajectories

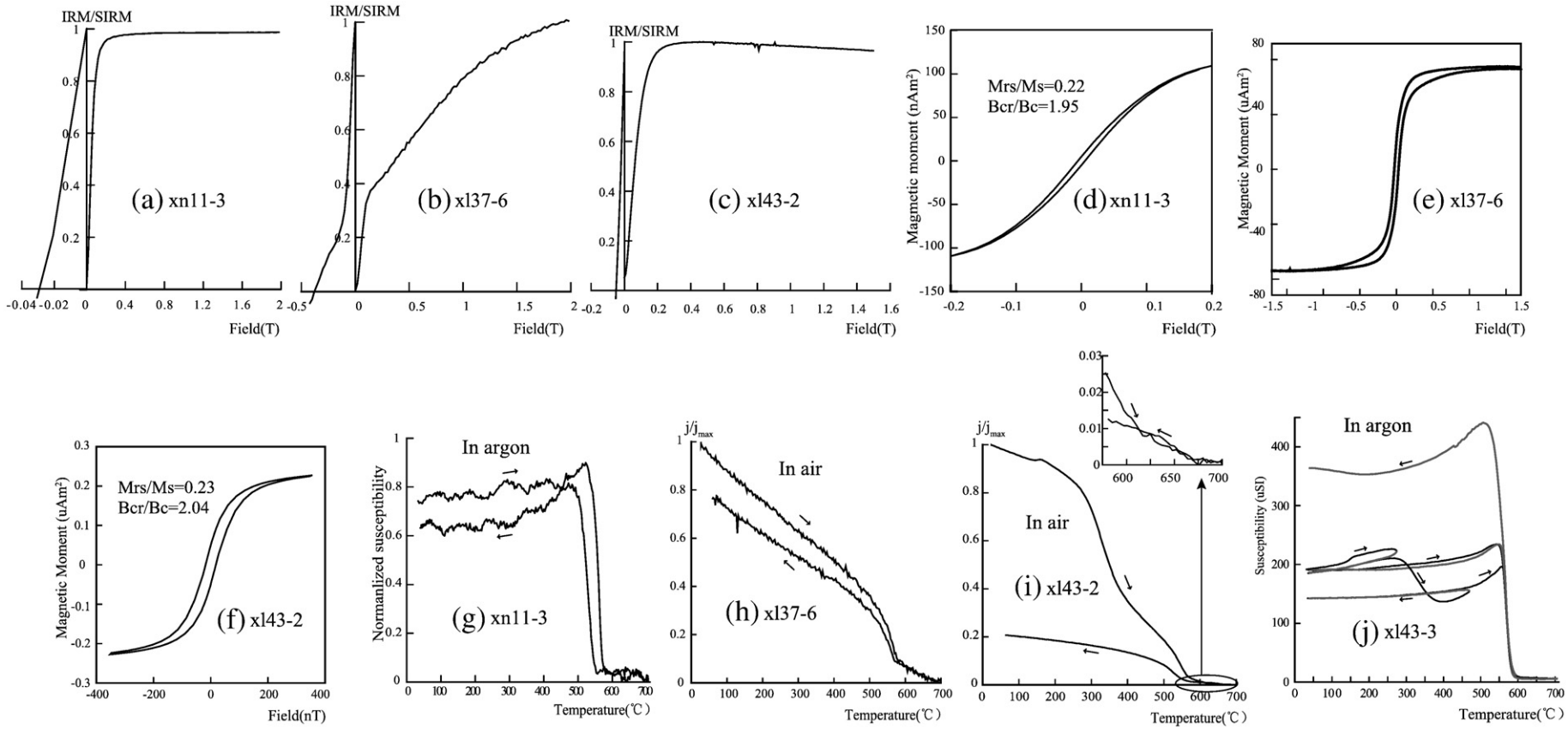

Fig. 3. Rock magnetic results for representative Linzizong volcanic and sedimentary samples from the Linzhou and Namling basins, Lhasa Block. (a–c) Acquisition curves of IRM and back-field demagnetization curves of saturation IRM; (d–f) hysteresis loops; and (g–j) thermomagnetic behaviors (*k*–*T* or *J*–*T* curve). The *J*–*T* curves were measured in an air atmosphere whilst the *k*–*T* measurements were carried out in an argon atmosphere.

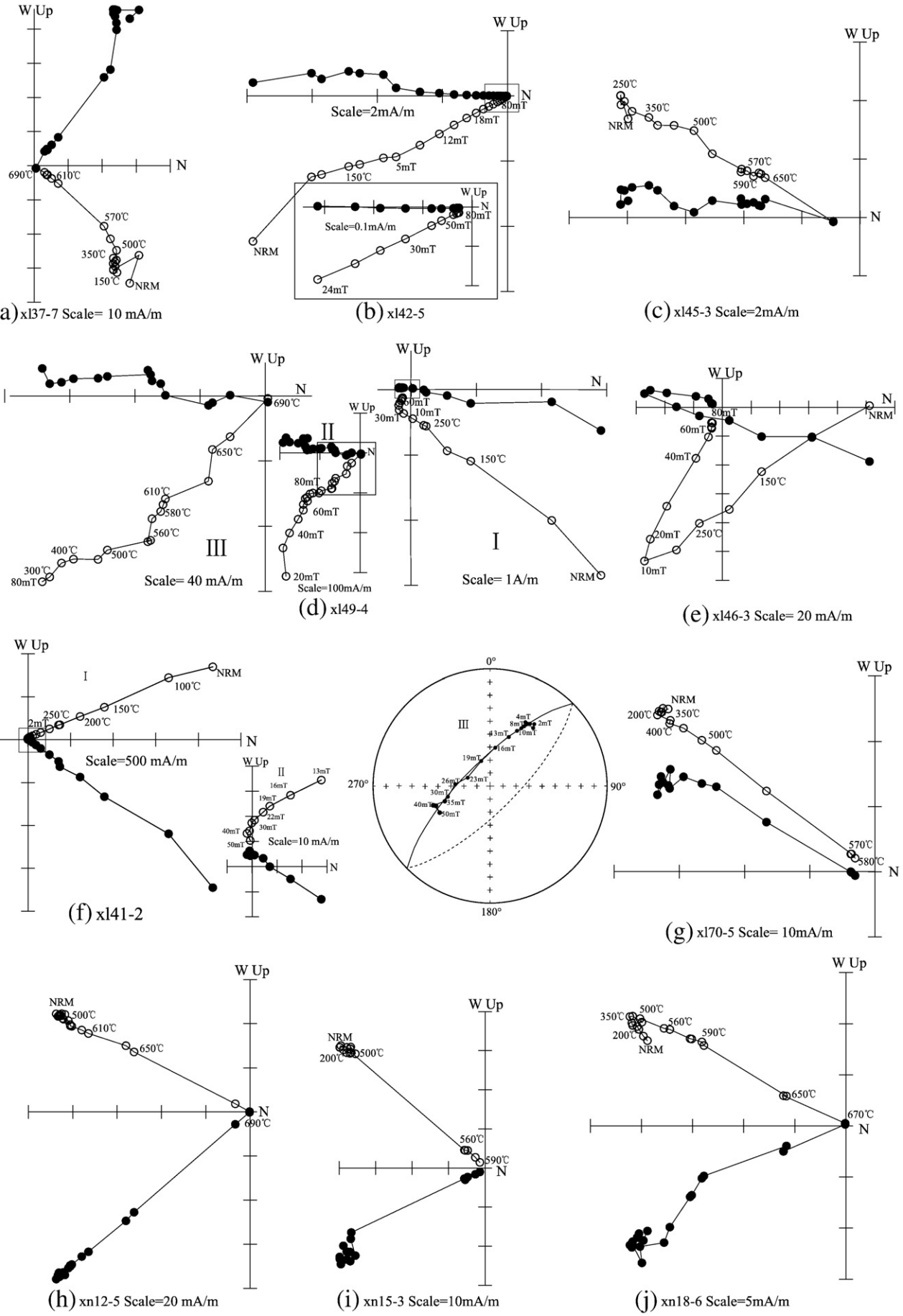
W Up
N
690℃
610℃
570℃
500℃
350℃
150℃
NRM
(a) xl37-7 Scale= 10 mA/m
Scale=2mA/m
80mT
18mT
12mT
5mT
150℃
Scale=0.1mA/m
50mT
30mT
24mT
(b) xl42-5
250℃
350℃
500℃
570℃
590℃
650℃
(c) xl45-3 Scale=2mA/m
III
II
I
Scale= 40 mA/m
Scale=100mA/m
Scale= 1A/m
(d) xl49-4
(e) xl46-3 Scale= 20 mA/m
Scale=500 mA/m
Scale=10 mA/m
(f) xl41-2
0°
90°
180°
270°
(g) xl70-5 Scale= 10mA/m
(h) xn12-5 Scale=20 mA/m
(i) xn15-3 Scale=10mA/m
(j) xn18-6 Scale=5mA/m

Table 1
Summary of paleomagnetic results of the ChRM from the Dianzhong Formation, Linzhou and Namling basins of the Lhasa Block.

Site ID	Lithology	φ_s (°N)	λ_s (°E)	Strike/dip	n/n_0	R/N	D_g (°)	I_g (°)	D_s (°)	I_s (°)	κ	α_{95} (°)	φ_p (°)	λ_s (°)
Tangbaqiao profile, Namling Basin, Shigatse														
xn12	Andesites	29.7936	89.2355	298/21	7/7	7/0	139.4	−18.8	144.4	−10.2	62.4	7.7	−48.4	150.0
xn13	Andesites	29.7928	89.2357	291/34	6/6	6/0	144.2	−24.4	151.2	−3.7	664.6	2.6	−50.9	139.0
xn14	Tuffaceous dacites	29.7791	89.2364	265/31	7/7	7/0	157.9	−28.2	160.1	1.7	379.9	3.1	−54.0	124.6
xn15	Tuffaceous dacites	29.7791	89.2364	273/24	7/7	7/0	160.2	−37.0	164.4	−14.5	282.0	3.6	−63.2	125.5
xn16	Tuffaceous dacites	29.7788	89.2364	291/29	6/7	6/0	158.9	−36.9	167.5	−13.7	367.2	3.5	−64.3	119.0
xn17	Tuffaceous dacites	29.7745	89.2367	265/31	5/7	5/0	158.4	−42.6	162.3	−12.6	64.5	9.6	−61.3	128.2
xn18	Tuffaceous dacites	29.7741	89.2368	299/31	5/5	5/0	163.5	−23.1	168.0	−0.2	290.0	4.5	−58.2	112.5
Sub-mean					7/7	7/0	154.2	−30.4			45.5	9.0		
									159.6	−9.0	47.9	8.8		
Nagagunba–Xiagunba profile and Chongga profile, Linzhou Basin, Lhasa														
xl40	Andesites	29.9588	91.1960	234/33	5(1)/6	5/0	190.3	−45.0	176.7	−19.1	35.1	13.1	−69.6	100.6
xl41+42	Andesites	29.9588	91.1960	236/19	7(5)/14	6/1	181.7	−51.0	172.6	−34.6	27.1	11.8	−77.2	124.5
xl43#	Andesites	29.9588	91.1960	236/19	5/6	1/4	14.0	51.0	1.6	36.7	16.0	19.7	−80.4	82.2
xl44#	Andesites	29.9598	91.1960	210/19	2/5	0/2	240.6	4.8	240.6	−5.0	–	–	26.5	194.6
xl45	Tuffaceous andesites	29.9601	91.1909	190/29	5(1)/9	5/0	184.5	−22.8	173.8	−17.3	30.0	14.2	−68.1	107.8
xl46	Andesites	29.9645	91.1960	268/34	7/7	7/0	191.6	−52.9	186.6	−19.5	121.4	5.5	−69.1	72.7
Xl47#	Andesites	29.9648	91.1956	268/34	3/7	3/0	176.1	37.0	173.3	71.0	93.8	12.8	−4.4	95.0
xl48	Andesites	29.9645	91.1836	268/34	6/6	6/0	187.8	−42.7	185.3	−9.1	144.1	5.6	−64.1	79.0
xl49	Andesites	29.9645	91.1836	282/31	8/8	8/0	195.4	−46.5	194.4	−15.6	92.1	5.8	−64.2	56.8
xl68+69	Tuffs	29.9617	91.1400	211/21	5/7	5/0	204.0	−30.0	194.0	−25.6	60.7	9.9	−69.0	50.0
xl70	Tuffs	29.9617	91.1400	261/34	7/8	7/0	211.0	−27.6	200.3	−25.6	98.9	6.1	−65.0	38.1
Sub-mean					8/11	11/0	193.9	−40.2			34.4	9.6		
									185.5	−21.1	43.8	8.5		
Group-mean					15/18	15/0	174.3	−36.9			14.6	10.4	66.0	284.9
									173.5	−14.8	19.8	8.8	$K=21.3$	$A_{95}=8.5$
Fold test:														
(1) Watson and Enkin's Test (1993): the optimum concentration is achieved at 86.5 ± 12.3% unfolding;														
(2) McElhiny's Test (1964): $N=15$, $ks/kg=1.356<F[28,28]=1.883$ of the grouping of the ChRM, at 95% confidence limits, indicative of indeterminate fold test;														
(3) McFadden's Test (1990): $N=15$, in-situ $\xi_2=6.712$, tilt-corrected $\xi_2=0.991$, statistical threshold $\xi=4.510$ at 95% confidence level, indicative of a positive fold test.														

Abbreviations are: site ID, site identification; Strike/dip, strike azimuth and dip of bed; n/n_0, number of samples joined the calculation/demagnetized, number showing in the parentheses indicate number of remagnetization circles used; R/N, samples show reversed and normal polarity; D_g, I_g (D_s, I_s), declination and inclination of direction in-situ (after tilt correction); φ_s, λ_s, latitude and longitude of the sampling site; φ_p, λ_p, latitude and longitude of corresponding virtue geomagnetic pole (VGP) in stratigraphic coordinates.
Group-mean direction calculated following transfer of site-mean directions to the sampling location of 91.2°E, 30.0°N, Linzhou Basin.
#Sites discarded due to larger uncertainties ($\alpha_{95}>15°$) or significant dispersions from the other observations.

(Fig. 4f) and in these cases site-mean directions of the HTC were calculated by combining remagnetization great circles with directional observations using the McFadden and McElhinny (1988) method. Together with the HTC from the upper part of the formation, 8 out of the 11 sites collected provide a group-mean direction for the HTC of $D=193.9°$, $I=-40.2°$ ($\alpha_{95}=9.6°$) before and of $D=185.5°$, $I=-21.1°$ ($\alpha_{95}=8.5°$) after tilt correction with slight improvement of data grouping following tilt correction yielding the ratio $ks/kg=1.27$ (Fig. 7c–d). This fold test is inconclusive (McElhinny, 1964; McFadden, 1990) due to the small variation in bedding attitudes within the basin. The other three sites (xl43, 44, and 47) yielded site-mean directions with either larger uncertainties, or with discernible deviations from the majority, and were excluded from further analysis (Table 1).

4.1.2. Nianbo Formation

From the lower part of this formation, 58 drill-cores in 6 sites (xl50-55) were collected from the vicinity of the Xiagunba Temple (Fig. 2a). Progressive thermal demagnetization showed that 38 out of 48 specimens demagnetized could define a LTC within the temperature interval between ~100 and 300/400 °C following removal of a viscous overprint in the initial stage of demagnetization (Fig. 5a–b, d). However, the HTC directions could only be defined from 19 specimens with unblocking temperatures of either ~580 °C (Fig. 5a) or >630 °C (Fig. 5b). For the remaining specimens, an intermediate temperature component (ITC) is significantly present at temperatures between ~300/400 °C and 580 °C (Fig. 5d) and sometimes the ITC may exist up to ~650 °C; in these cases the HTC was often difficult to define due to either the low intensity of the NRM or obliteration of the ITC. Nevertheless, the demagnetization trajectories mostly followed great circles and permitted the isolation of a remagnetization great circle within the temperature interval between ~300 °C and <670° (Fig. 5d). Accordingly, site-mean directions for the HTC in this unit, which are predominantly of normal polarity with only one site (xl50) showing reversed polarity, were obtained by the combination of remagnetization great circles and directional observations following the McFadden and McElhinny (1988) method (Table 2). It is noteworthy that a total of 26 out of the 38 specimens demagnetized isolated an ITC at temperatures between 300/400 °C and <650 °C and in these cases the HTC could not be accurately defined. The ITC is predominantly of normal polarity with only one specimen showing an approximately antipodal direction and it yields a group-mean direction of $D=3.0°$, $I=36.9°$ ($\alpha_{95}=6.5°$) before and $D=358.1°$, $I=9.1°$ ($\alpha_{95}=7.0°$) after tilt correction with slight deterioration in grouping ($kg/ks=20.0/17.5$). Noting that the ITC has approximately similar directions to the site-mean directions for the HTC both before and after tilt correction, we speculate that it likely resulted from a biased HTC. The nature for the low and high temperature components will be analyzed later together with those isolated from the middle part of this formation.

For the middle part of this formation, 4 sites in tuffs (xl56) and limestones (xl57-59) were collected from the vicinity of the village of Renjigang (Fig. 2a). Progressive thermal demagnetization of 32

Fig. 4. Typical orthogonal and stereographic vector plots illustrating progressive thermal or AF demagnetization structures for Linzizong rocks from the Linzhou Basin. Orthogonal directions (Zijderveld plots) are plotted in geographic coordinates; whilst stereographic directions are plotted in stratigraphic coordinates; solid and open symbols represent vector endpoints projected onto horizontal or vertical planes, respectively.

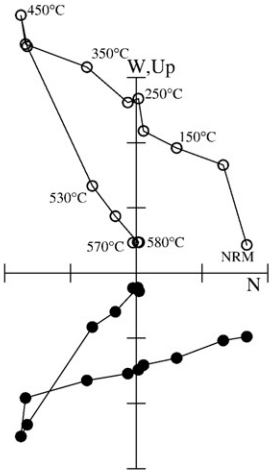

(a) x150-6 Scale=0.5mA/m

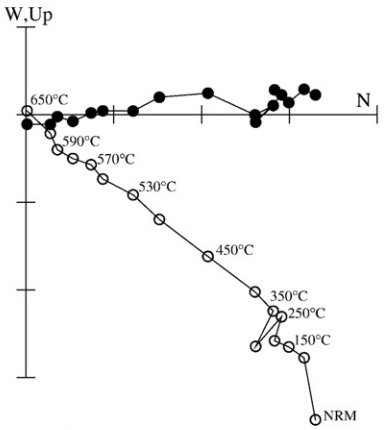

(b) x153-4 Scale=0.5mA/m

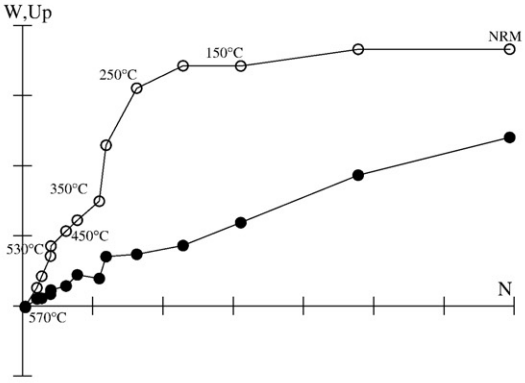

(c) x158-2 Scale=2mA/m

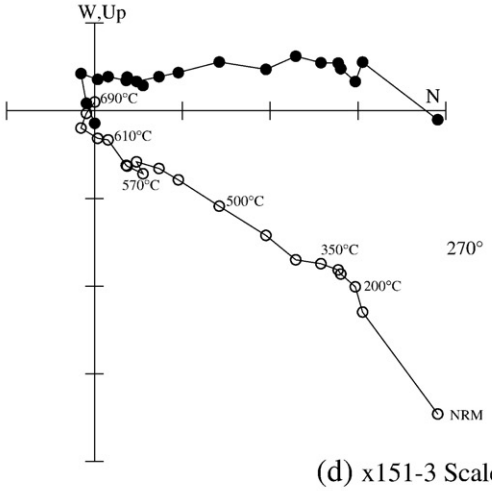

(d) x151-3 Scale=0.5mA/m

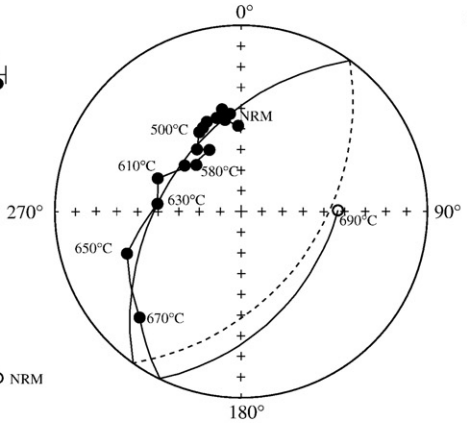

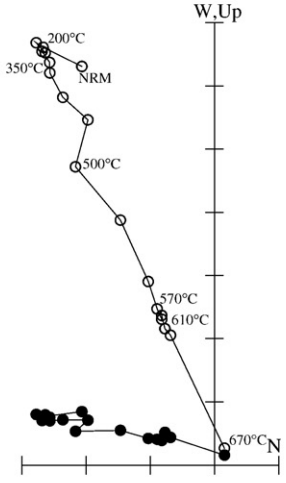

(e) x157-3 Scale=1mA/m

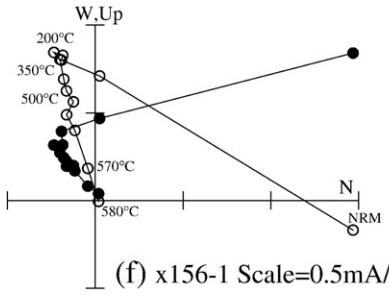

(f) x156-1 Scale=0.5mA/m

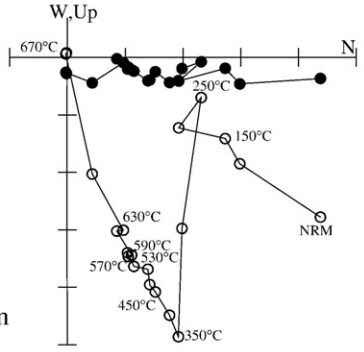

(g) x159-5 Scale=0.05mA/m

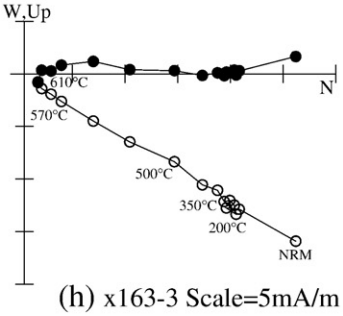

(h) x163-3 Scale=5mA/m

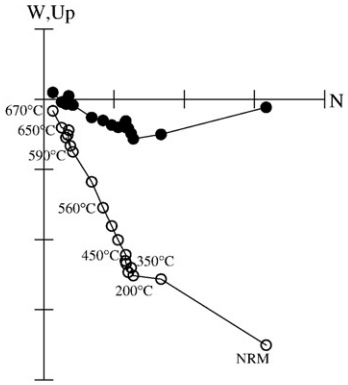

(i) x166-3 Scale=4mA/m

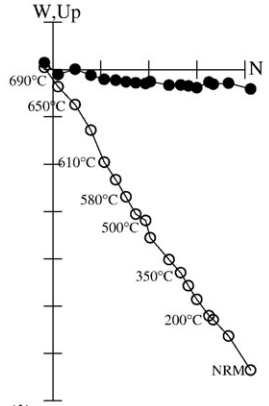

(j) xn3-2 Scale=0.5mA/m

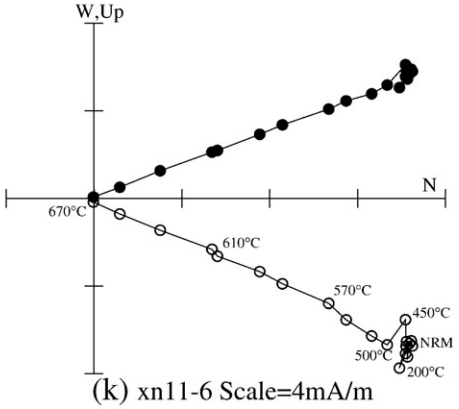

(k) xn11-6 Scale=4mA/m

Table 2
Summary of paleomagnetic results of the ChRM from the Nianbo and Pana formations from the Linzhou and Namling basins, Lhasa Block.

Site ID	Lithology	φ_s (°N)	λ_s (°E)	Strike/dip	n/n_0	R/N	D_g (°)	I_g (°)	D_s (°)	I_s (°)	κ	α_{95} (°)	φ_p (°)	λ_s (°)
Tangbaqiao–Jiare profile, Namling Basin, Shigatse														
xn01	Tuffs	29.8195	89.2329	310/42	5/7	0/5	3.5	30.9	9.2	−4.7	51.1	10.8	56.6	252.3
xn02	Tuffs	29.8193	89.2337	291/31	6/8	6/0	158.5	−62.4	178.4	−35.8	71.1	8.0	−79.9	97.9
xn03	Sandstone	29.8192	89.2338	235/39	7/7	0/7	354.0	54.2	342.4	18.0	117.1	5.6	63.6	311.5
xn04	Tuffaceous sandstone	29.8190	89.2339	235/39	2/7	0/2	21.9	71.5	345.0	38.9	–	–	74.4	332.5
xn05#	Sandstone	29.8122	89.2360	296/23	4(3)/7	0/4	338.1	41.7	348.5	24.6	36.1	15.5	70.0	303.9
xn06	Marlaceous sandstone	29.8122	89.2360	308/40	6/7	0/6	351.5	46.8	7.1	14.8	28.3	12.8	66.7	251.2
xn07	Marlaceous sandstone	29.8122	89.2360	185/11	5(5)/7	0/5	336.6	19.6	333.7	14.1	43.0	11.8	56.5	322.0
xn08	Sandstones	29.8115	89.2359	212/38	5/7	0/5	0.3	46.4	340.7	20.3	99.7	7.7	63.6	316.2
xn09#	Sandstones	29.8115	89.2359	163/31	5(4)/7	0/5	340.3	20.2	327.4	17.2	18.4	18.3	53.0	331.4
xn10	Tuffs	29.8115	89.2359	50/26	7/7	0/7	351.4	15.5	358.9	36.9	911.1	2.0	80.7	275.6
xn11	Tuffs	29.8105	89.2361	96/25	7/7	0/7	339.9	23.3	331.1	45.0	753.2	2.2	64.4	359.1
Sub-mean					9/11	0/9	350.9	41.7			14.0	14.3		
									350.1	25.0	15.9	13.3		
Xiagunba, Renjigang and Gulu profiles, Linzhou Basin, Lhasa														
xl50	Tuffaceous sandstones	29.9800	91.1803	241/24	5(1)/8	5/0	193.0	−58.0	178	−38.0	113.9	7.2	−81.2	103.4
xl51	Tuffaceous sandstones	29.9800	91.1803	241/24	8(7)/8	0/8	357.3	33.8	353.1	11.9	95.4	5.7	65.2	287.7
xl52	Conglomerate tuffs	29.9796	91.1795	226/35	7(7)/8	0/7	5.2	35.6	354.6	9.9	44.9	9.1	64.5	283.8
xl53	Tuffs	29.9796	91.1795	248/26	8(2)/8	2/6	353.6	34.3	351.0	9.1	54.1	7.6	63.2	291.4
xl54	Sandstones, limestones	29.9796	91.1795	247/40	6(3)/8	0/6	14.5	38.8	5.4	4.7	85.2	7.3	61.9	259.7
xl55	Sandstones, limestones	29.9789	91.1793	286/33	8(3)/8	0/8	14.5	47.4	15.0	14.4	30.4	10.2	63.3	236.3
xl56	Tuffs	29.9761	91.1676	256/44	8/8	8/0	232.0	−84.4	173.0	−43.5	72.2	6.1	−82.3	146.3
xl57	Argillaceous limestones	29.9761	91.1676	256/44	8/8	8/0	201.0	−74.9	176.0	−33.1	139.8	4.7	−77.5	109.1
xl58#	Limestones	29.9761	91.1676	256/44	8/8	6/2	290.9	−83.7	173.9	−49.3	11.3	17.2	−84.7	184.8
xl59	Argillaceous limestones	29.9761	91.1676	249/70	5/8	2/3	11.0	81.9	343.0	13.1	55.1	10.4	61.7	309.0
Sub-mean					9/10	3/6	6.8	54.9			13.8	14.4		
									356.5	20.1	23.8	10.8		
Gulu–Nianbo profile, Linzhou, Lhasa														
xl60	Tuffs													
	Tuffaceous andesites	30.0193	91.1411	272/29	6/7	0/6	3.5	34.2	3.2	5.2	413	3.3	62.4	264.2
xl61	Tuffaceous andesites	30.0193	91.1411	276/26	8/8	0/8	6.1	30.3	6.1	4.3	580.5	2.3	61.5	258.3
xl62	Andesites, tuffs	30.0193	91.1411	274/24	8/8	0/8	4.3	34.2	4.3	10.2	696.1	2.1	64.8	261.0
xl63	Tuffs	30.0186	91.1411	266/26	7/7	0/7	357.9	33.0	357.6	7.0	189.1	4.4	63.4	276.5
xl64##	Conglomerate tuffs	30.0122	91.1403	327/22	8/8	0/8	7.1	51.6	21.4	35.2	40.6	8.8	67.9	204.9
xl65##	Conglomerate tuffs	30.0122	91.1403	327/22	8/8	0/8	293.1	79.4	27.9	71.8	45.5	8.3	57.0	119.3
xl66	Tuffs	30.0114	91.1403	272/37	6/9	0/6	12.2	72.4	5.8	35.6	100.9	6.7	78.4	242.8
xl67#	Tuffs	30.0101	91.1403	289/24	6/6	0/6	329.6	85.6	11.7	63.0	718.7	2.5	72.8	120.5
Sub-mean					5/8	0/5	3.7	40.6			20.6	17.2		
									3.3	12.3	36.0	12.9		
Group-mean					23/29	4/19	0.1	46.7			13.9	8.4	70.6	281.0
									355.9	20.2	20.2	6.9	K = 33.2	A_{95} = 5.3

Fold test:
(1) Watson and Enkin's Test (1993): the optimal concentration is achieved at 66.88 ± 5.0% unfolding level.
(2) McElhiny's Test (1964): $N = 23$, $ks/kg = 1.453 < F[44,44] = 1.632$ of the grouping of the ChRM, at 95% confidence level, indicative of indeterminate fold test;
(3) McFadden's test (1990): $N = 23$, in-situ $\xi_1 = 8.976$, tilt-corrected $\xi_1 = 5.393$ statistical threshold $\xi = 5.583$ at 95% confidence level, indicative of a positive fold test.

The abbreviations are the same as for Table 1.
Sites were discarded due to a significant collapse of the sampling strata, see text for more information.

specimens yielded simple trajectories with clear separation of two magnetic components (Fig. 5c, 5e–g). The LTC was completely removed by temperatures ~250–350 °C and the succeeding HTC was well isolated between temperatures of ~400–570/580 °C in sites xl56 and xl58 and in a few specimens from sites xl57 and xl59, or between ~450–670 °C in most specimens from sites xl57 and xl59. The HTC is predominantly of reversed polarity with a few specimens from sites xl58-59 showing normal polarity (Table 2). As a result, the LTC could be defined from 21 specimens by more than three demagnetization steps and as with those defined from sites xl50-55 in the lower part of this formation, it is also of single normal polarity and distributed around the local present geomagnetic field (PGF) direction. Together with the LTCs defined at sites xl50-55, a total of 59 out of 70 specimens demagnetized yielded a group-mean of $D = 4.6°$, $I = 54.0°$, $\alpha_{95} = 4.9°$ before tilt adjustment with a meaningful reduction of data grouping after tilt correction defined by a ratio $kg/ks = 1.88$ (Fig. 6c–d). Thus, the LTC might be a viscous or recent overprint. For the HTC, site xl58 yielded a site-mean observation with larger uncertainty (Table 2) and was discarded from further analysis, the remaining 3 sites and those HTC components defined from sites xl50-55 yielded a group-mean direction of $D = 6.8°$, $I = 54.9°$ ($\alpha_{95} = 14.4°$) before and $D = 356.5°$, $I = 20.1°$ ($\alpha_{95} = 10.8°$) after tilt correction. The grouping of the dataset is slightly improved after tilt correction with the ratio $ks/kg = 1.725$ (Fig. 8a–b) and an optimal concentration at 98.3 ± 18.0% unfolding (Watson and Enkin, 1993). Following application of the McFadden (1990) fold test, the result is positive with in-situ $\xi_2 = 4.228$, tilt-corrected $\xi_2 = 1.533$, and statistically critical $\xi = 3.497$ at the 95% confidence level. This indicates that the HTC defined from sites xl50-59 is pre-folding and possibly primary.

However, the HTC from these sites failed a reversal test due to some marked differences in inclination between the normal and reversed directions following tilt correction (Fig. 8b). Although some

Fig. 5. Typical orthogonal and stereographic vector plots illustrating progressive thermal demagnetization structures for Linzizong rocks from the Namling Basin. Symbols etc. are the same as for Fig. 4.

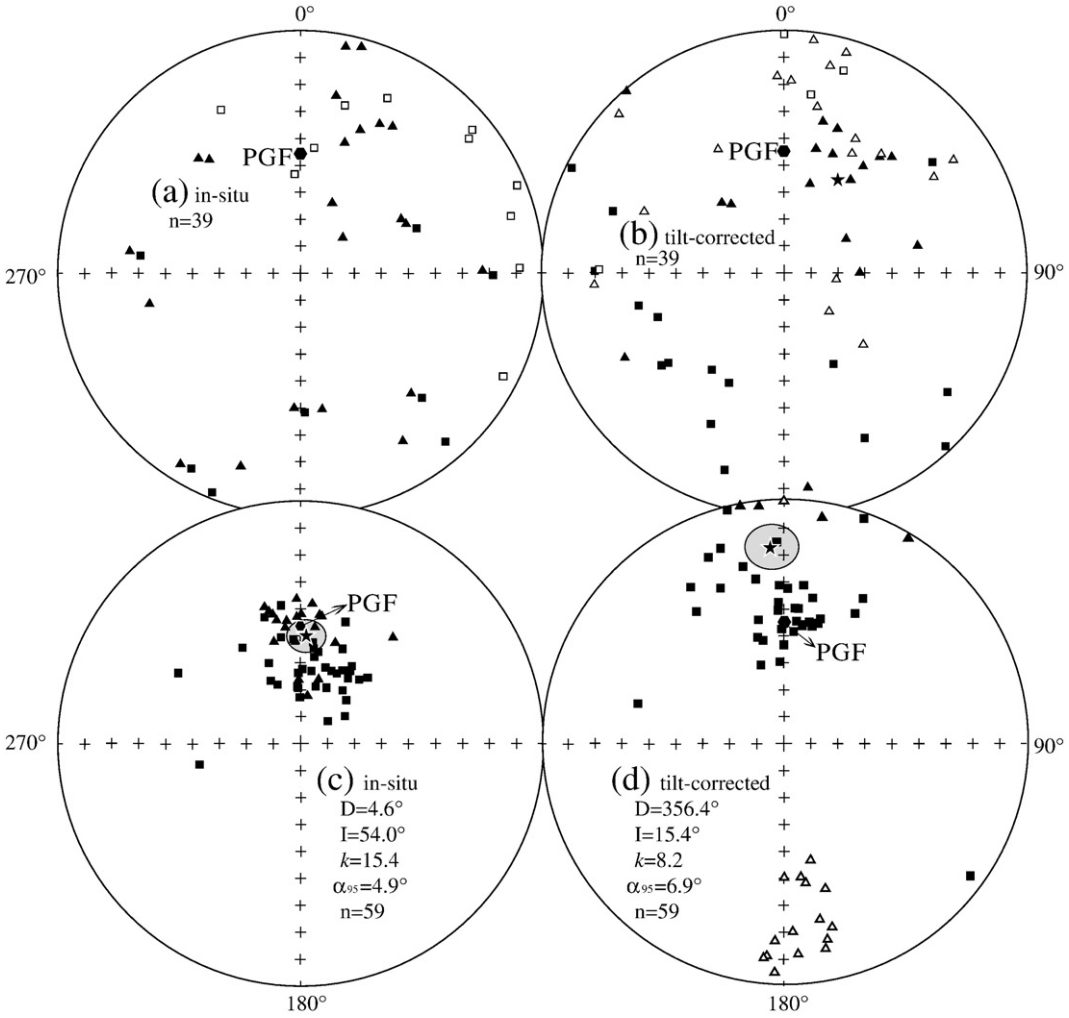

Fig. 6. Equal-area projections of directions of low temperature components (LTCs) isolated from the Dianzhong (a–b) and Nianbo (c–d) formations in the Linzhou Basin before and after tilt correction. Solid/open symbols represent positive/negative inclinations; stars indicate the overall-mean directions with 95% confidence limits. Triangles and squares in (a) and (b) indicate LTC directions isolated from the lower part (xl37-39) and the middle and upper parts (xl40-49 and xl68-70) of the Dianzhong Formation, respectively; triangles and squares in (c) and (d) indicate LTC directions from the lower (xl50-55) and upper (xl56-59) parts of the Nianbo Formation, respectively; PGF indicates the direction of present geomagnetic field.

in-situ site-mean directions are clustered around the PGF (Fig. 8a), the positive fold test result from the HTC precludes the possibility of a recent overprint. We therefore prefer to interpret the significant difference in inclination between the normal and reversed tilt-corrected directions in terms of an age difference; however, we qualify this interpretation by noting that we have no clear evidence to show that the recent overprint (LTC) has been completely removed from the specimens with normal polarity owing to the necessary use of remagnetization great circles (Table 2). Indeed, three site-mean directions with reversed polarity (Fig. 8b) have tilt-corrected inclinations compatible with those isolated from the younger strata (Pana Formation, Fig. 9d). Noting (i) that the Nianbo Formation experienced a protracted formation of ~10 Ma (from ~60 to 50 Ma), and (ii) that some sites are composed of tuffs or tuffaceous sandstones, we consider that some significant apparent polar wander may have caused the above significant difference in inclination between the normal and reversed directions, and consequently resulted in the negative reversal test.

4.1.3. Pana Formation

In total, 68 drill-cores were collected from 8 sites (xl60-67) in the upper part of this formation in the vicinity of the village of Gulu (Fig. 2a); samples are composed of tuffs, ignimbrites and tuffaceous andesites (Fig. 2c and Table 2). Thermal demagnetization trajectories for sites xl60-63 and xl67 are relatively simple and yield a slight drop of NRM intensity at temperatures below ~300 °C followed by a straightforward decay to the origin (Fig. 5h). On the other hand, thermal demagnetization from the remaining 3 sites (xl64-66) identified both LTC and HTC components: the LTC was mostly removed by temperatures of ~350–400 °C whilst the HTC was generally isolated at temperatures between ~450–500 °C and 650–690 °C (Fig. 5i). As a result, the LTC could only be isolated from a few specimens from sites xl64-66; however, the dispersed distribution of these LTCs either in-situ or after tilt correction precludes further analysis of their origin. The HTC was readily isolated from 59 specimens with the majority subtracted at temperatures between 350/400 °C and 690 °C and the minority (xl63) between ~450 °C and 590 °C. However, further field examination found that two sites (xl64, 65) had been collected from strata incorporating evidence for collapse and they have thus been discarded from further analysis. Site xl67 yielded an anomalous site-mean observation similar to that isolated from the collapsed site xl65 and has also been excluded. The remaining 5 sites have a group-mean direction of $D=3.7°$, $I=40.6°$ ($\alpha_{95}=17.2°$) before and of $D=3.3°$, $I=12.3°$ ($\alpha_{95}=12.9°$) after tilt correction with insignificant change in directional grouping (Fig. 8e–f) due to small variations in bedding attitudes of the sampled strata. However, when combined with component directions isolated from the

Nianbo Formation in the same basin (sites xl50-59), a positive fold test (McFadden, 1990) results from a total of 14 sites with in-situ $\xi_2 = 7.264$, tilt-corrected $\xi_2 = 2.532$, and statistically critical $\xi = 4.358$ at 95% confidence level.

4.2. Namling Basin

4.2.1. Dianzhong Formation

Thermal demagnetization trajectories from specimens collected from the Jiare profile (xn12-18, Fig. 2b) are relatively straightforward and two components were isolated from most specimens following removal of a viscous overprint at initial stages of demagnetization (Fig. 4h–j). However, the LTC could not be well isolated from some specimens at temperatures between ~100 °C and 300–400 °C due to only a slight drop of the NRM intensity in this demagnetization interval (Fig. 4h–j). The HTC generally appeared above ~500 °C and was unblocked by 670–690 °C in the majority, and by ~590 °C in the minority, of the collection (Fig. 4h–j). The HTC components have mostly SSE declinations with shallow inclinations following tilt correction, and the 7 site-mean observations have a Fisherian group-mean direction of $D = 154.2°$, $I = -30.4°$ ($\alpha_{95} = 9.0°$) before and $D = 159.6°$, $I = -9.0°$ ($\alpha_{95} = 8.8°$) after tilt correction (Fig. 7e–f). The grouping of data is therefore very slightly increased with tilt adjustment; the ratio $ks/kg = 1.233$ however, remains less than the critical value (2.69) for $N = 7$ at the 95% confidence level (McElhinny, 1964) showing that directional groupings are statistically indistinguishable before and after the tilt adjustment.

4.2.2. Nianbo Formation

A total of 116 drill-cores from 11 sampling sites (xn1-11) were collected from the Tangbaqiao profile (Fig. 2b) with the samples comprising mainly tuffs, sandstones, and tuffaceous sandstones (Fig. 2d and Table 2). Thermal demagnetization resolved the presence of two magnetic components (Fig. 5j–k) although the LTC could not always be well isolated due to slight decrease of the NRM intensity in the low temperature demagnetization stage (Fig. 5k). However, most sandstone specimens yielded straightforward demagnetization trajectories decaying to the origin with unblocking temperatures of ~670–690 °C (Fig. 5j) and the presence of a characteristic component. The LTC was generally completely removed by temperatures of ~300–

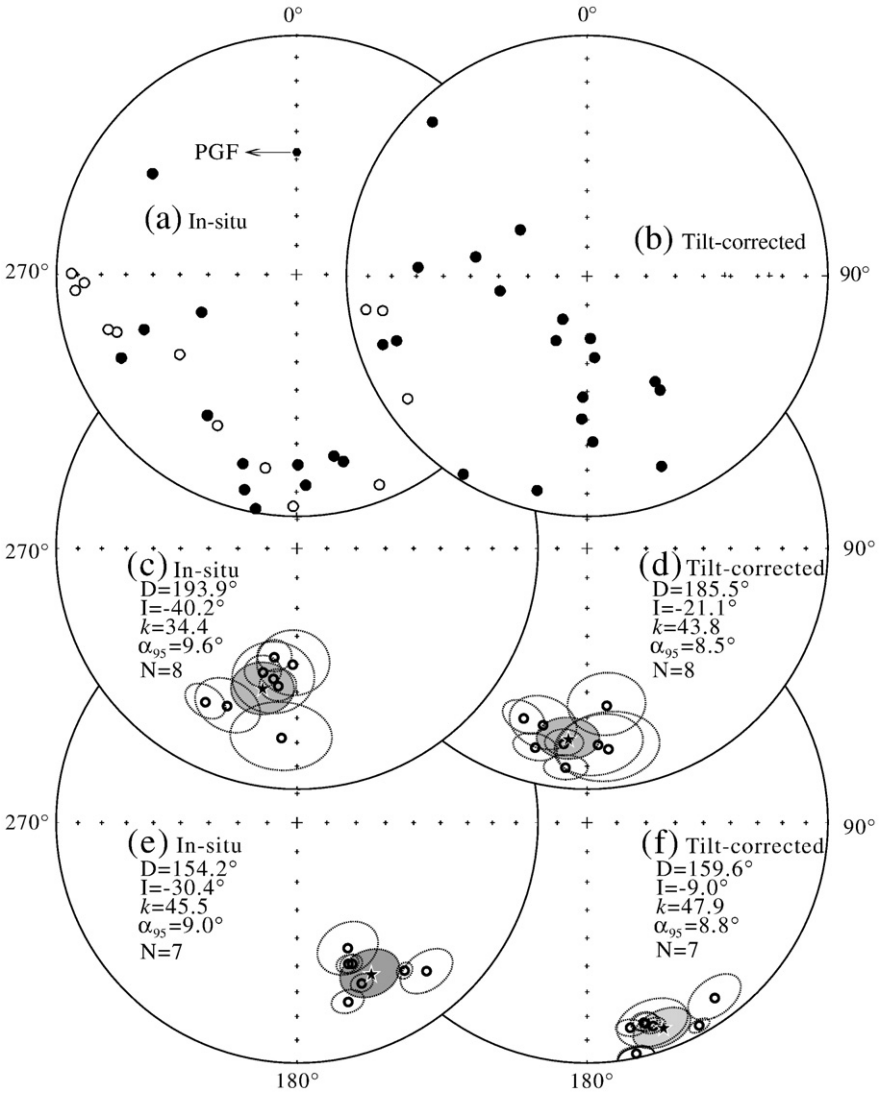

Fig. 7. Equal-area projections of directions of high temperature components (HTCs) isolated from the Dianzhong Formation before and after tilt correction. (a–b), HTC directions isolated from the lower part of the Dianzhong Formation (xl37-39) in the Linzhou Basin; (c–d), site-mean directions subtracted from the middle and upper parts of Dianzhong Formation in the Linzhou Basin; (e–f), site-mean directions isolated from the Dianzhong Formation in the Namling Basin. Symbols etc. are the same as for Fig. 6.

450 °C whilst the characteristic HTC was mostly unblocked by ~630–690 °C (Fig. 5j–k). Nevertheless, the HTC directions could not be well isolated from sites xn5, xn7 and xn9 where high temperature demagnetization trajectories exhibited a great circle distribution. By combining remagnetization great circles with directional observations (McFadden and McElhinny, 1988) approximate site-mean directions could be calculated for these three sites (Table 2). Excluding two sites xn5 and xn9 with larger uncertainties (Table 2), the remaining 9 sites yielded a group-mean direction of $D=350.9°$, $I=41.7°$ ($\alpha_{95}=14.3°$) before and $D=350.1°$, $I=25.0°$ ($\alpha_{95}=13.3°$) after tilt correction with slight improvement in directional grouping identified by the ratio $ks/kg=1.11$ (Fig. 8c–d). However, application of the McFadden (1990) fold test to the HTC yields a positive test result with in-situ $\xi_2=5.793$, tilt-corrected $\xi_2=4.361$, and critical $\xi=4.849$ at 99% confidence level (Table 2) and this test implies that the HTC may have a pre-folding origin.

4.3. Summary of paleomagnetic results

The low, and sometimes similar, bedding attitudes in some sampling profiles (Tables 1 and 2) mean that the standard palaeomagnetic fold test often has little or no significance. For this reason we include all available site-mean characteristic directions from both the Linzhou and Namling basins and evaluate them by time period. For the Dianzhong Formation, with the exception of three sites in breccias and tuffs (xl37-39) from the lower part of the formation which failed to isolate meaningful site-mean HTCs, 18 out of the 21 sites yielded meaningful site-mean HTC directions with a predominance of reversed polarity (Fig. 9a–b and Table 1). With the exception of three sites (xl43, 44, and 47) with larger uncertainties or significant deviations from the majority of the collection, 15 sites yield a Fisherian average direction of $D=174.3°$, $I=-36.9°$ ($\alpha_{95}=10.4°$) before and $D=173.5°$, $I=-14.8°$ ($\alpha_{95}=8.8°$) after tilt correction; the

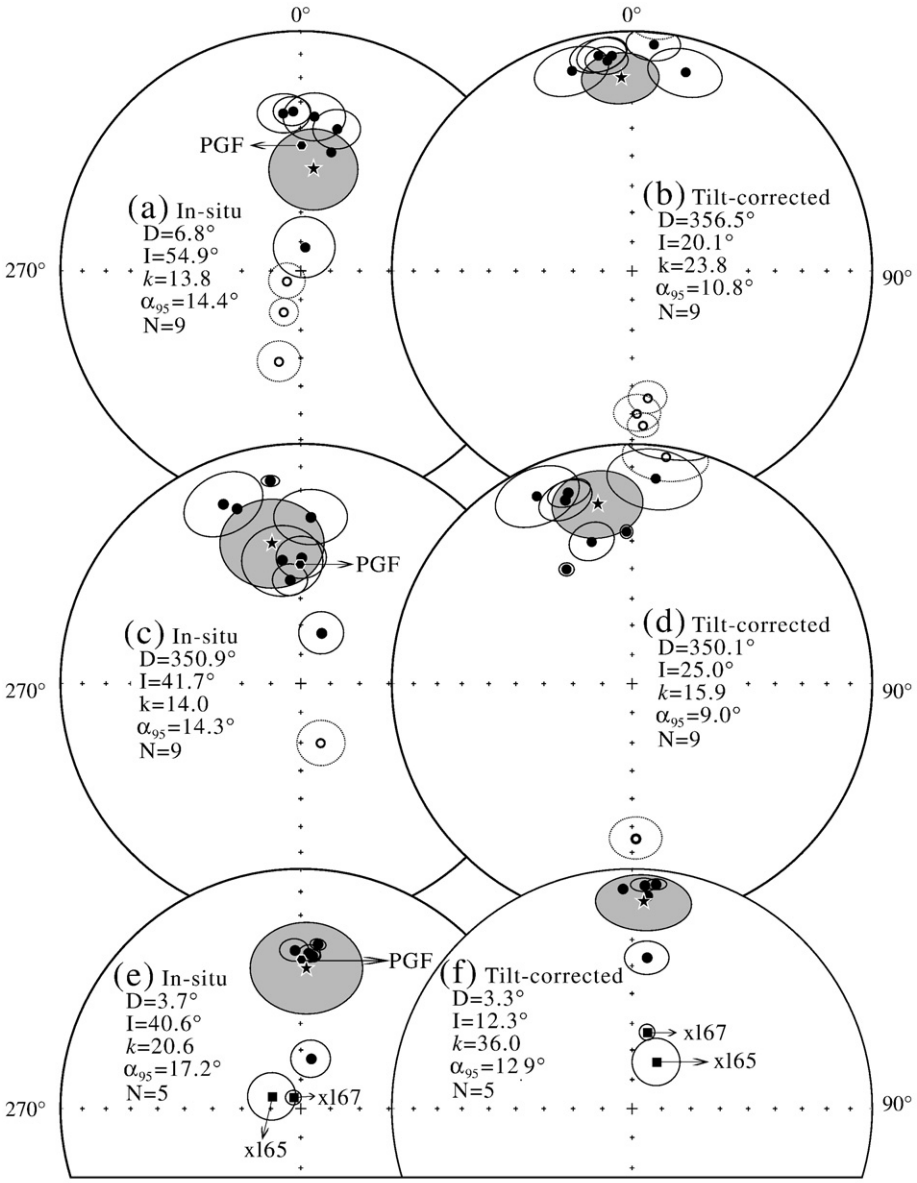

Fig. 8. Equal-area projections of site-mean directions of high temperature components (HTCs) isolated from the Nianbo and Pana formations before and after tilt correction. (a–b), The Nianbo Formation in the Linzhou Basin; (c–d), the Nianbo Formation in the Namling Basin; (e–f), the Pana Formation in the Linzhou Basin. Directions of two discarded sites xl67 and xl65 (solid squares) are also shown in the plot. Symbols etc. are the same as for Fig. 6.

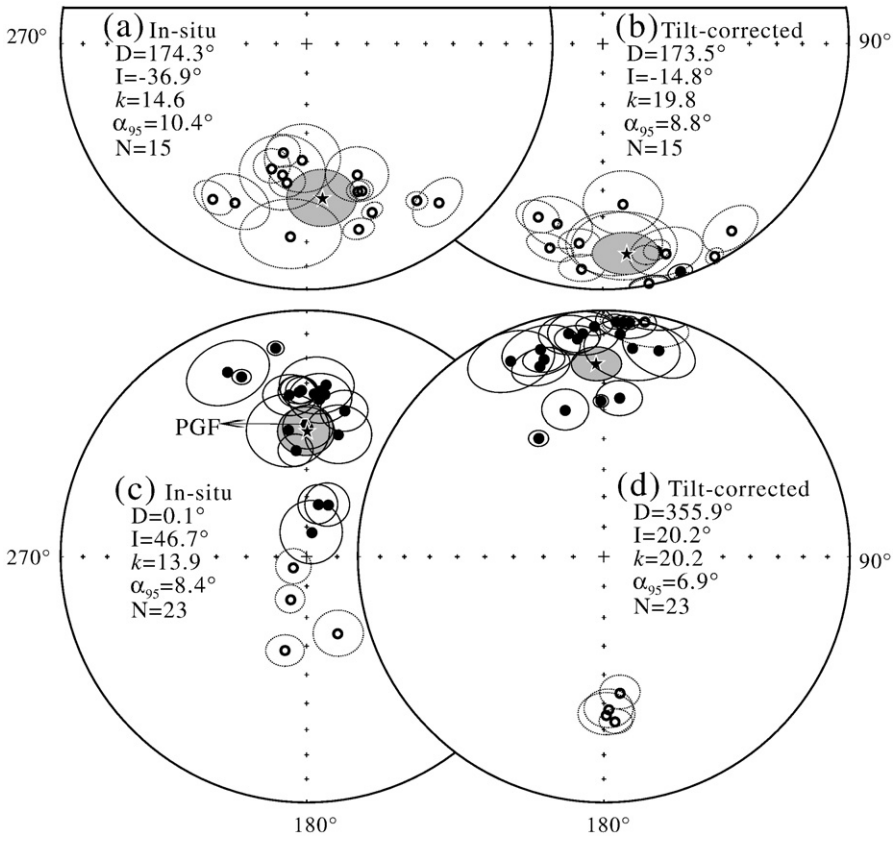

Fig. 9. Equal-area projections of site-mean directions of high temperature components (HTCs) from both the Linzhou and Namling basins of the Lhasa Block before and after tilt correction. (a–b), The Dianzhong Formation; (c–d), the Nianbo and Pana formations. Symbols etc. are the same as for Fig. 6.

grouping of the dataset is thus improved to some extent after tilt correction indicated by the ratio $ks/kg = 1.36$ (Fig. 9a–b), although this improvement does not have statistical significance (McElhinny, 1964). With the application of McFadden's (1990) fold test the HTC yields a positive fold test at the 95% confidence level (Table 1), suggesting that this HTC has a pre-folding origin.

Similarly, for the Pana and Nianbo formations, site-mean directions of the HTC were successively isolated from 29 sites (Table 2). With the exception of two sites (xl64 and xl65) where the outcrop was evidently not in-situ, three sites (xn5, xn9 and xl58) showing larger uncertainties ($\alpha_{95}>15°$) and one site (xl67) exhibiting large deviations from the majority of the collection, 23 sites yield a group-mean direction of $D = 0.1°$, $I = 46.7°$ ($\alpha_{95} = 8.4°$) before and $D = 355.9°$, $I = 20.2°$ ($\alpha_{95} = 6.9°$) after tilt correction (Table 2). The grouping of this dataset is slightly improved after tilt correction as defined by the ratio $ks/kg = 1.453$ (Fig. 9c–d) but remains less than the threshold at the 95% confidence level (McElhinny, 1964). With application of McFadden's (1990) fold test the dataset has a positive result at 95% confidence level (Table 2). The rock magnetic experiments (Fig. 3) and demagnetization characteristics (Figs. 4 and 5) identify the HTC from the Dianzhong, Nianbo, and Pana volcanic rocks as resident in magnetite and/or oxidation-induced hematite; formation of the latter is usually attributable to deuteric oxidation and it has the effect of improving the remanence stability of a primary or quasi-primary remanence. Hence the HTCs in this study most likely merit an interpretation as primary remanence.

5. Paleogeographic location of the Lhasa Block in the Paleogene

Large-scale northward convergence and lateral tectonic extrusion has occurred at the site of the Himalaya–Tibetan plateau within central Asia and the southern margin of Eurasia as a consequence of the India–Asia collision and post-collisional indentation of India into Asia (e.g. Tapponnier et al., 1982; Achache et al., 1984; Besse et al., 1984; Patriat and Achache, 1984; England and Searle, 1986; Dewey et al., 1988; Le Pichon et al., 1992; Avouac et al., 1993; Chen et al., 1993; Yang and Besse, 1993). As a consequence of the very wide distribution of this deformation, the well-constructed master APW paths for stable Eurasia (e.g. Acton, 1999; Besse and Courtillot, 2002; Schettino and Scotese, 2005; Torsvik et al., 2008) cannot be used to determine paleopositions of the Lhasa Block either before or after the India–Asia collision. Accordingly, paleopositions of the leading edge of Asia before or during the initial contact can only be determined by direct paleomagnetic analysis within the Lhasa Block.

The new paleomagnetic poles obtained from this study for the middle and upper parts of the Dianzhong Formation and the Nianbo and Pana formations of the Lhasa Block (Tables 1 and 2) indicate a paleolatitude of ~10°N for the southernmost margin of the Asian continent during formation of the Linzizong Group. In the light of recent geochronological advances in constraining the ages of the Linzizong volcanic rocks (Fig. 2c–d and Mo et al., 2003; Zhou et al., 2004; Dong et al., 2005), the Lhasa Block (reference site: 30.0°N, 91.2°E) is therefore predicted to have lain at paleolatitudes of 6.6°N ± 8.5° during formation of the Dianzhong Formation (~64–60 Ma) and at 10.8°N ± 5.3° during formation of the Nianbo and Pana formations (~60–44 Ma). Comparison of these two paleopoles from the Linzizong Group (Fig. 10a) indicates that the Lhasa Block was subjected to an insignificant clockwise rotation of 2.4 ± 9.4° and latitudinal flattening of 5.4 ± 9.0° during formation of the Linzizong Group. This implies that the Lhasa Block experienced no paleomagnetically-detectable movement during formation of the Linzizong Group and remained essentially stationary at ~10°N during the time period embracing the interval ~64 and 44 Ma.

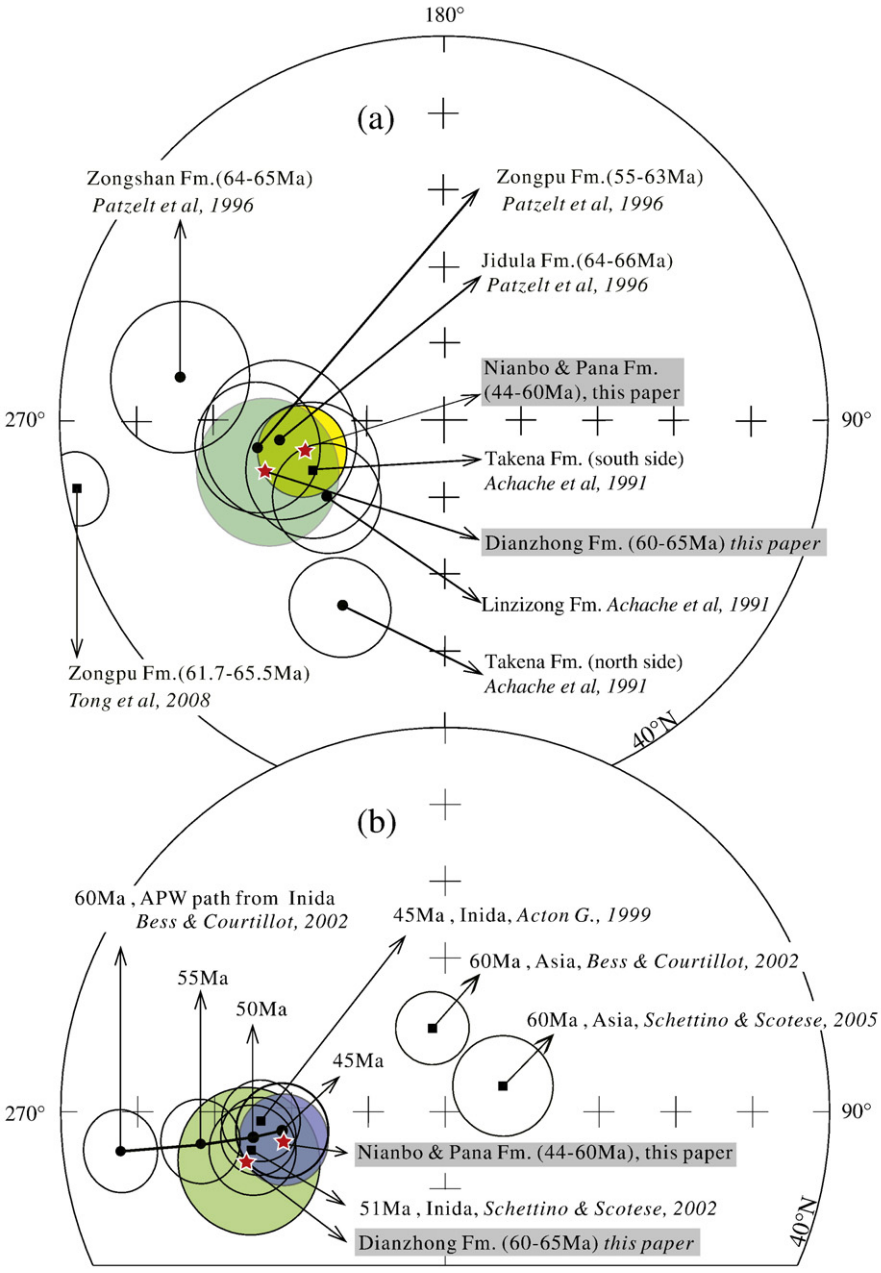

Fig. 10. Equal-area projections showing comparisons between (a) late Cretaceous and Paleogene paleomagnetic poles from the Himalayan and Lhasa blocks and (b) new paleomagnetic poles from the Linzizong Group in the Lhasa Block (stars) and the master APW path for India (circles) during the interval 60–45 Ma (Besse and Courtillot, 2002). Some other reference poles (squares) for both India and Asia are also included in the plot. Paleopoles are plotted onto the Northern Hemisphere with 95% confidence limits.

This view agrees very well with the preliminary paleomagnetic studies on the Linzizong volcanic rocks performed in the 1980's (Zhou et al., 1990; Achache et al., 1991) during which Linzizong andesite and welded tuff specimens were collected at 8 sites in the Linzhou Basin and yielded a paleolatitude of 13.5°N ± 6.5° for this same sector of the Lhasa Block.

Achache et al. (1991) further reported a paleomagnetic result from the Takena red sediments in the Lhasa Block with the Takena Formation paleontologically assigned to the Albian–Aptian (Jaeger et al., 1982). Although an intercontinental relative rotation of ~15° may have happened within the Lhasa Block along the Nyainqentanglha strike–slip fault in the vicinity of Yangbajain, the Albian–Aptian paleopole suggests a paleolatitude of 11.5°N ± 6.2° for the Lhasa Block at the same reference site. Thus, the Lhasa Block may have remained at low latitudes of ~10°N and been subject to no significant latitudinal motion during the interval between deposition of the Takena Formation during Albian–Aptian times (~125–100 Ma) and formation of the Linzizong Group between ~64 and 44 Ma. The insignificant latitudinal movement of the southern leading edge of Asia during this protracted interval suggests that collision-induced large-scale northward convergence within the Himalaya–Tibetan plateau and its hinterland (e.g. Chen et al., 1993; Yin and Harrison, 2000; Johnson, 2002; Huang et al., 2005a, 2006) occurred after formation of the Linzizong Group (<44 Ma).

Given that onset of the India–Asia collision occurred no later than ~50 Ma (Section 6), the essential quiescence of the Lhasa Block during formation of the Linzizong Group (~64–44 Ma) further supports the conclusion that subduction of Indian lithosphere occurred beneath

the Lhasa Block; this has been suggested from geophysical studies of crust and lithospheric structure beneath the Himalaya–Tibetan plateau (e.g. Powell and Conaghan, 1973; Barazangi and Ni, 1982; Zhao et al., 1993, 2001; Owens and Zandt, 1997; Kind, 2002). Since northward motion of India continued to be quite rapid until about 20–30 Ma (Acton, 1999), significant northward movement of the Lhasa Block, the southernmost tectonic unit of the Asian continent, should be recorded from the Linzizong Group (~64–44 Ma) in the absence of subduction. In the event, the absence of such motion would appear to be the consequence of subduction of Indian lithosphere beneath Asia.

6. Initial time of the India–Asia collision

Given that the position of the Lhasa Block, the southernmost tectonic unit of the Asian continent, is now defined by paleopoles in late Cretaceous and Paleogene times, two paleomagnetic arguments may be used to constrain the onset of the India–Asia collision.

Firstly, a direct comparison of coeval paleomagnetic data from both sides of the IYSZ could provide crucial constraints on the time of initial contact between the leading edges of India and Asia. Patzelt et al. (1996) reported paleomagnetic results from the Zongshan (~65–71 Ma), Jidula (~63–66 Ma), and Zongpu formations (~55–63 Ma) developed in the Gamba/Duela sedimentary basin within the Himalayan Block (Fig. 10a). The northern margin of the Himalayan Block (reference site: 30.0°N, 91.2°E) may therefore have been located at 4.7°S ± 4.4°, 7.5°N ± 4.8° and 4.8°N ± 3.8° during deposition of these formations with the qualification that these results are likely to be influenced by inclination-shallowing which would give them a southerly bias. The comparable paleolatitudes from the Linzizong Group in the Lhasa Block are 6.6°N ± 8.5° (~64–60 Ma) and 10.8°N ± 5.3° (~60–44 Ma). Thus paleolatitude estimates from both sides of the IYSZ during the interval 64–55 Ma are essentially compatible at the 95% confidence level and indicate that the initial India–Asia collision might have occurred at the beginning of, or before, formation of the Linzizong Group. Noting that the Lhasa Block may have remained essentially stationary between the late Cretaceous and the mid-Eocene (this paper and Achache et al., 1991), the paleomagnetic results from the Zongshan Formation (~65–71 Ma) in Gamba (Patzelt et al., 1996) could imply a paleolatitudinal difference of more than ten degrees between the leading edges of the Himalayan and Lhasa blocks during the interval of ~65–71 Ma; this would suggest an initial contact between India and Asia no earlier than the *K*/*P*g boundary at ~65 Ma.

The view that onset of the India–Asia collision occurred around the *K*/*P*g boundary is supported by substantial geological evidence (Klootwijk et al., 1992; Briggs, 2003; Rage, 2003). In particular, in the middle part of the IYSZ, the Linzizong Group developed within the Linzhou Basin is in contact with the underlying late Cretaceous Shexing Formation with a significant unconformity: the rocks developed just under the contact surface comprise of red sandstones with lenses of gravel composed of oblate pebbles, whilst the rocks above the contact comprise a suite of gray tuffaceous andesites belonging to the lower part of the Dianzhong Formation. In the vicinity of Kaibu, Nagagunba and Chongga in the Linzhou Basin, many xenoliths of red Shexing sandstones can be found within the Linzizong volcanic rocks and are recorded by a number of studies (Liu, 1993; Dong et al., 2005; Lee et al., 2007). Regional geological expeditions have found that the unconformity between the Linzizong volcanic rocks and underlying Shexing red sediments in Linzhou is a common feature of the Linzizong Group developed in other areas of the Lhasa Block (TRGST, 1990, 1991; GSTAR, 2002; Huang et al., 2005a; Pan et al., 2005). Mo et al. (2003, 2006, 2008) further proposed that the tectonic event corresponding to this unconformity is likely to record the onset of the India–Asia collision. In addition, simultaneous, large-scale deformation occurred on both sides of the IYSZ around the *K*/*P*g boundary and also supports the view that the two continents collided during these times (Ding et al., 2005, 2007).

However, the above discussion is in conflict with a recent paleomagnetic study in the Dingri area of the Himalayan Block (Tong et al., 2008) where a high temperature ChRM isolated from the lower part of the Zongpu Formation (61.7–65.5 Ma) indicates a paleolatitude of 15.6°S ± 4.0° (reference site: 28.42°N/86.50°E) for the Himalayan Block in early Danian time. In the light of this new paleoposition for the Danian Himalayas (Tong et al., 2008) the initial contact between India and Asia should have occurred no earlier than ~61.7 Ma. Moreover, a primary remanence isolated from Eocene limestones (57 ± 1 Ma) in the Dingri area (Besse et al., 1984) also indicated a depositional paleolatitude of 2.5°S ± 4° (reference site: 29°N/87°E) for the northernmost Indian continent, suggesting that this northernmost margin of the Indian plate was still in the Southern Hemisphere at ~57 Ma leaving no possibility for contact with the Lhasa Block at around the *K*/*P*g boundary.

Aitchison and coworkers (e.g. Aitchison et al., 2000, 2007; Aitchison and Ali, 2001; Ali and Aitchison, 2008) have recently proposed that onset of the India–Asia collision occurred during Priabonian times at ~35 Ma. This revised India–Asia collision model proposed a very late initial contact between India and Asia and implied a much higher paleolatitude of ~30°N for the southernmost margin of the Asian continent during the interval 55–35 Ma (Figs. 11–13 of Ali and Aitchison, 2008). This further implies that initial contact between India and Asia should have occurred at the present position of the IYSZ and that no noticeable post-collisional crustal thickening and shortening has occurred in the Tibetan plateau and central Asia. Clearly, these two hypotheses are in conflict with the paleomagnetic results from the Linzizong Group (this paper and Zhou et al., 1990; Achache et al., 1991), which suggest a much lower paleolatitude for the Lhasa Block during the period ~64–44 Ma. We therefore conclude that the younger India–Asia collision model (Aitchison et al., 2000, 2007; Ali and Aitchison, 2008) is unlikely. On the other hand, comparison between our new paleopoles for the Linzizong Group and the master APW path for stable India (Besse and Courtillot, 2002) indicates that Paleogene paleopoles for the Lhasa Block are significantly separated from the coeval reference pole for India at 60 Ma. They are, however, indistinguishable with coeval reference poles from India at 50 and 45 Ma (Fig. 10b). This suggests that onset of the India–Asia collision occurred no later than 50 Ma. This is consistent with the lower limit of the initial collision time identified from analysis of sedimentary provenances on both sides of the IYSZ (Ding et al., 2005).

Secondly, if the size and shape of the Indian plate could be accurately predicted prior to the India–Asia collision, the initial time of the collision might be determined from comparison of paleopositions between the northernmost edge of Greater India and the Lhasa Block during late Cretaceous–Paleogene times. However, although the study of Greater India has a long history of over 80 years and a large number of geological, geophysical and geochemical studies, geoscientists are still uncertain of the actual size of Greater India. Noting that large-scale tectonic deformation and northward subduction beneath the Asian continent may have happened at the northern margin of Greater India during the collision, it is not surprising that there are a variety of models for Greater India (Ali and Aitchison, 2005 and references therein).

As shown in Fig. 11a, paleopositions for the northernmost margin of India during the period of 80–30 Ma can be readily calculated from the master APW path (Besse and Courtillot, 2002). Direct comparison in paleolatitudes between the two leading edges of Greater India and the Lhasa Block implies an overlap of paleolatitudes at ~50 Ma, indicative of an initial India–Asia collision no later than ~50 Ma. However, geophysical studies have shown that Greater India may have subducted beneath the Lhasa Block at a shallow angle of ~10° into the north of the IYSZ, and the front edge approaching the BNSZ ~400 km north of the IYSZ (Zhao et al., 1993, 2001; Owens and Zandt, 1997; Kind, 2002). Hence Greater India may have a northern extension of ~500 km beyond its present northern margin, and paleopositions for the northern margin

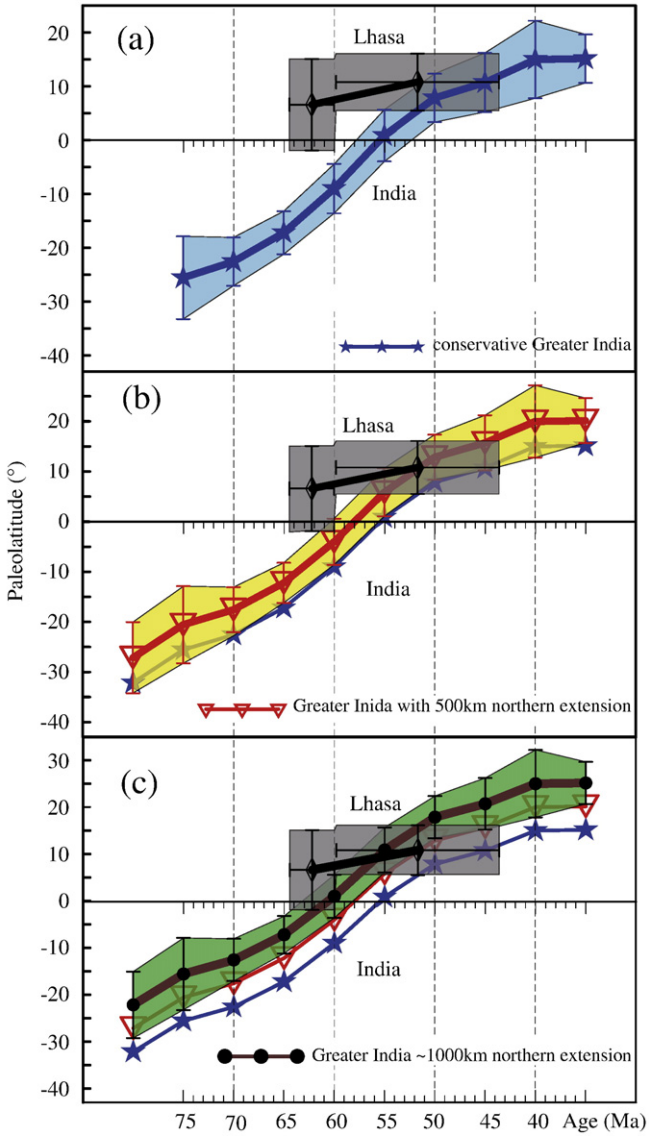

Fig. 11. Time-dependent paleolatitudes for the northernmost edge of Greater India and the southernmost edge of the Lhasa Block during the period embracing the interval 80 and 35 Ma. Paleolatitudes for the Lhasa Block are computed from the two Paleogene paleopoles in this study; whilst paleolatitudes for the northernmost edge of Greater India are computed from the master APW path for India (Besse and Courtillot, 2002) and different models for Greater India: Greater India in plot (a) is the most conservative model without any considerations of either continental subduction or tectonic shortening in the Himalayas; whilst Greater India in plot (b) assumes a continental subduction of ~500 km (~5° paleolatitudes) beyond the present northernmost margin of the Indian plate; Greater India used in plot (3) is according to the most acceptable model proposed by Ali and Aitchison (2005) where Greater India is constrained to have a northern extension of ~950 km (~10° paleolatitudes) beyond its present north-central margin. All the paleolatitudes are computed at the reference site of 30.0°N, 91.2°E.

of this inferred Greater India are shown in Fig. 11b. Clearly, paleolatitudes for the northern leading edge of Greater India are statistically indistinguishable from those for the Lhasa Block at ~55 Ma, again suggesting that the initial India–Asia contact had occurred by ~55 Ma. This estimation is not only in agreement with the dramatic reduction of the northward drift velocity of India at ~55 Ma (Klootwijk et al., 1992), but is also compatible with an initial collision time at 55–60 Ma as identified from paleomagnetic studies within the Himalayas (e.g. Klootwijk and Peirce, 1979; Tong et al., 2008). Thus, if no obvious latitudinal convergence occurred between the IYSZ and the MBT in the Himalayas (e.g. Tong et al., 2008), then onset of the India–Asia collision should have occurred no later than ~55 Ma.

The northern margin of the Indian plate consists of a number of tectonic units incorporated within the Kangma–Longzi, the Tethyan Himalaya, the High Himalaya, and the Low Himalaya (Pan et al., 2005) separated from each other from north to south by the IYSZ, STDS, MCT and MBT (Fig. 1). On the other hand, the highest mountain (Mt. Everest) and the deepest valley (Yarlung–Zangbo Grand Canyon) of the Himalaya–Tibetan plateau are both located within a narrow area between the MBT and IYSZ (~300-km-wide, >2500-km-long). Within this zone strongly undulating topography and the world's most spectacular fold-and-thrust belt are very likely to have accommodated large-scale post-collisional crustal shortening and thickening. Accordingly, most models for Greater India have assumed a tectonic shortening of at least several hundreds of kilometers in the Himalayas (Veevers et al., 1975; Besse et al., 1984; Besse and Courtillot, 1988; Dewey et al., 1989; Treloar and Coward, 1991; Klootwijk et al., 1992; Le Pichon et al., 1992; Patzelt et al., 1996; Matte et al., 1997; Mattauer et al., 1999). However, no consensus has yet been reached on the magnitude of tectonic shortening in the Himalayas. Ali and Aitchison (2005) proposed a Greater India model from bathymetric features in the Indian Ocean and a Gondwanan reconstruction immediately prior to rifting and break-up of the western and eastern segments of the supercontinent (~160 Ma). In this model Greater India is constrained to have a northern extension of ~950 km beyond its present north-central margin which includes a ~500-km-wide segment of Indian lithosphere subducted into the southern part of the Asian continent, and another ~500-km-wide Indian lithosphere portion accommodated by the spectacular fold-and-thrust belts in the Himalayas. As shown in Fig. 11c, paleolatitudes for the northernmost edge of this Greater India are statistically indistinguishable from those from the Lhasa Block at 55–60 Ma; this suggests that the initial India–Asia contact occurred at 55–60 Ma or earlier. Together with paleopositions for the Lhasa Block during the interval ~64–44 Ma (Section 5) and the master APW paths for the Indian and Eurasian plates (Besse and Courtillot, 2002), we identify a stepwise approaching and colliding process between Greater India (Ali and Aitchison, 2005) and Eurasia during the period between 65 and 50 Ma (Fig. 12). It is clear that the initial contact between India and Asia most likely occurred between 55 and 60 Ma within low latitudes of the Northern Hemisphere. Since the northern leading edge of Greater India was still located in the Southern Hemisphere at ~65 Ma, this model does not permit an onset of the India–Asia collision prior to the *K/Pg* boundary.

7. Conclusions

Paleomagnetic study of the Linzizong volcanic rocks and intercalated sediments from the Linzhou and Namling basins in the Lhasa Block has yielded ChRMs from the Dianzhong Formation (~64–60 Ma) and the Nianbo and Pana formations (~60–44 Ma). These remanences reside in both volcanic and sedimentary rocks, pass a fold test, and are sometimes carried by oxidation-induced hematite permitting us to interpret them as quasi-primary remanences. The corresponding poles are located at 66.0°N, 284.9°E with $A_{95} = 8.5°$ for the Dianzhong Formation and at 70.6°N, 281.0°E with $A_{95} = 5.3°$ for the Nianbo and Pana formations. They indicate that the Lhasa Block experienced neither obvious tectonic rotation nor latitudinal motion during formation of the Linzizong Group within the interval ~64–44 Ma. Paleopositions of the Lhasa Block during formation of the Linzizong Group are also compatible with those identified from the Albian–Aptian Takena red sediments (Achache et al., 1991), further suggesting that the Lhasa Block may have remained essentially stationary at ~10°N during the Albian–Aptian to Danian–Lutetian interval; a large-scale post-collisional crustal shortening and thickening in the Tibetan plateau and central Asia is predicted to have occurred after formation of the Linzizong Group. A comparison between paleopositions for the Lhasa Block and those from the northern leading edge of the Indian plate estimated from either coeval

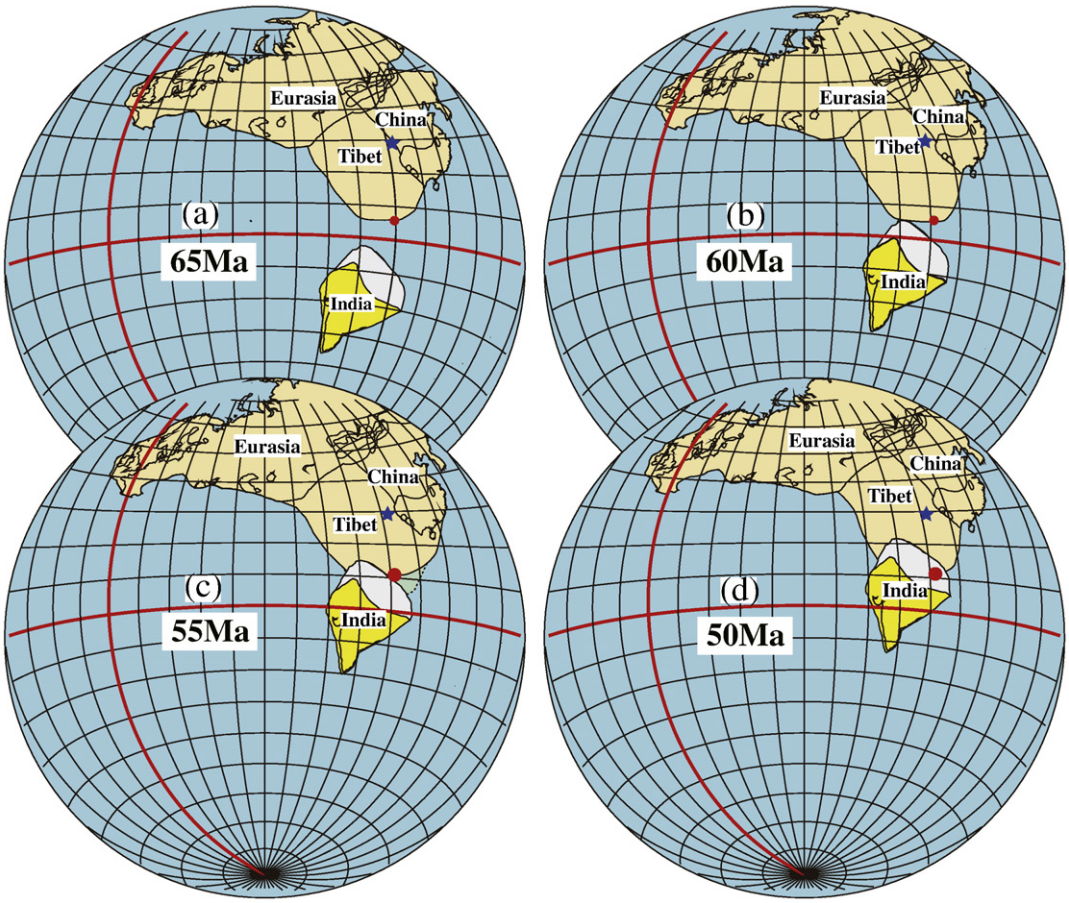

Fig. 12. Equal-area projections of paleopositions of the Indian and Eurasian continents during the period between 65 and 50 Ma in present geographic coordinates. The Indian continent is shown following the Greater India model of Ali and Aitchison (2005) and reference paleopoles for India (Besse and Courtillot, 2002); whilst the Eurasian continent is plotted according to the master APWP for stable Eurasia (Besse and Courtillot, 2002) and new paleopositions for the Lhasa Block in the southern leading edge of the continent. Stars indicate the location of the present Linzhou Basin (30°N, 91.2°E); solid cycles represent paleopositions of the southernmost margin of the Lhasa Block computed from the paleopoles for the Dianzhong Formation (a and b) and the Nianbo and Pana formations (c and d); the dashed line in (c) indicates the southernmost edge of Asia as defined from the paleopole of the Dianzhong Formation.

paleomagnetic data from the Himalayas (Patzelt et al., 1996; Tong et al., 2008), or from the master APW path for stable India (Besse and Courtillot, 2002), shows that initial contact between India and Asia occurred between ~50 and ~65 Ma. Also the Greater India model restricted by the Late Jurassic Gondwanan reconstruction and submarine topography of the SE Indian Ocean (Ali and Aitchison, 2005) suggests that onset of the India–Asia collision is most likely to have occurred at ~55–60 Ma.

However, we note that most discussions on the subject of onset of the India–Asia collision are still challenged by uncertainties about the shape and size of Greater India. Further combined paleontostratigraphic, magnetostratigraphic, and paleomagnetic investigations on the late Cretaceous–Paleogene marine successions developed in the Himalayas will be required to accurately determine paleopositions of the northern leading edge of the Indian plate. Also paleomagnetic studies to date have not been sufficiently comprehensive to address the significance of the inclination-shallowing contribution to the paleomagnetic studies (Tauxe and Kent, 2004). More extensive investigations will be required to assess the contributions of this effect and thereby refine quantitative estimates of paleolatitude.

Acknowledgements

We are grateful to Zhonghai Zhuang, Lianzhong Lu, Hongfei Liu and Zhenyu Li for field assistance and sincerely appreciate the throughout comments, suggestions, and criticisms of two journal anonymous reviewers, J.D.A Piper, and the editor. This work was supported by the Key Items of Knowledge Innovation Programs of the Chinese Academy of Sciences (KZCX2-YW-Q09-01) and the National Natural Science Foundation of China (40525013 and 40821091).

References

Achache, J., Courtillot, V., Zhou, Y.X., 1984. Paleogeographic and tectonic evolution of southern Tibet since middle Cretaceous time: new paleomagnetic data and synthesis. J. Geophys. Res. 89 (B12), 10311–10339.

Achache, J., Courtillot, V., Zhou, Y.X., 1991. Paleogeographic and tectonic evolution of southern Xizang (Tibet) since middle Cretaceous time: new paleomagnetic data and synthesis. In: Li, G., Yuan, X., Hirn, A. (Eds.), Geology of the Himalayas—Papers on Geophysics. Geol. Printing House, Beijing, pp. 201–244.

Acton, G.D., 1999. Apparent polar wander of India since the Cretaceous with implications for regional tectonics and True Polar Wander. Mem. Geol. Soc. India 44, 129–175.

Aitchison, J.C., Ali, J.R., 2001. When did the India–Asia collision really happen? Gondwana Res. 4, 560–561.

Aitchison, J.C., Zhu, B.D., Davis, A.M., Liu, J., Luo, H., Malpas, J.G., McDermid, I.R.C., Wu, H.Y., Ziabrev, S.V., Zhou, M.F., 2000. Remnants of a Cretaceous intra-oceanic subduction system within the Yarlung–Zangbo suture (southern Tibet). Earth Planet. Sci. Lett. 183, 231–244.

Aitchison, J.C., Ali, J.R., Davis, A.M., 2007. When and where did India and Asia collide? J. Geophys. Res. 112 (B05423), 1–21.

Ali, J.R., Aitchison, J.C., 2005. Greater India. Earth-Sci. Rev. 72, 169–188.

Ali, J.R., Aitchison, J.C., 2008. Gondwana to Asia: plate tectonics, paleogeography and the biological connectivity of the Indian sub-continent from the Middle Jurassic through latest Eocene (166–35 Ma). Earth-Sci. Rev. 88, 145–166.

Avouac, J.P., Tapponnier, P., Bai, M.X., You, H.Z., Wang, G.Q., 1993. Active thrusting and folding along the northern Tien Shan and late Cenozoic rotation of the Tarim relative to Dzungaria and Kazakhstan. J. Geophys. Res. 98, 6755–6804.

Barazangi, M., Ni, J., 1982. Velocities and propagation characteristics of Pn and Sn beneath the Himalayan arc and Tibetan Plateau: possible evidence for underthrusting of the Indian continental lithosphere beneath Tibet. Geology 10, 179–185.
Besse, J., Courtillot, V., 1988. Paleogeographic maps of the continents bordering the Indian Ocean since the Early Jurassic. J. Geophys. Res. 93 (B10), 11791–11808.
Besse, J., Courtillot, V., 2002. Apparent and true polar wander and the geometry of the geomagnetic field over the last 200 Myr. J. Geophys. Res. 107 EPM6~1-EPM6~31.
Besse, J., Corutillot, V., Pozzi, J.P., Westphal, M., Zhou, Y.X., 1984. Palaeomagnetic estimates of crustal shortening in the Himalayan thrusts and Zanbo suture. Nature 311, 621–626.
Briggs, J.C., 2003. The biogeographic and tectonic history of India. J. Biogeogr. 30, 381–388.
Brookfield, M.E., 1998. The evolution of the great river systems of southern Asia during the Cenozoic India–Asia collision: rivers draining southward. Geomorphology 22, 285–312.
Chang, C.F., Chen, N., Coward, M.P., et al., 1986. Preliminary conclusions of the Royal Society and Academia Sinica 1985 geotraverse of Tibet. Nature 323, 501–507.
Chen, Y., Cogne, J.P., Courtillot, V., Tapponnier, P., Zhu, X.Y., 1993. Cretaceous paleomagnetic results from western Tibet and tectonic implications. J. Geophys. Res. 98, 17981–17999.
Chung, S.L., Chu, M.F., Zhang, Y.Z., Xie, Y.W., Lo, C.H., Lee, T.Y., Lan, C.Y., Li, X.H., Zhang, Q., Wang, Y.Z., 2005. Tibetan tectonic evolution inferred from spatial and temporal variations in post-collisional magmatism. Earth-Sci. Rev. 68, 173–196.
Clark, M.K., Schoenbohm, L.M., Royden, L.H., et al., 2004. Surface uplift, tectonics, and erosion of eastern Tibet from large-scale drainage patterns. Tectonics 23 2002TC001402.
Day, R., Fuller, M., Schmidt, V.A., 1977. Hysteresis properties of titanomagnetites: grain size and composition dependence. Phys. Earth Planet. Inter. 13, 260–267.
Dewey, J.F., Shackleton, R.M., Chang, C., Sun, Y., 1988. The tectonic evolution of the Tibetan Plateau. Philos. Trans. R. Soc. London, Ser. A 327, 379–413.
Dewey, J., Cande, S., Pitman, W.C., 1989. Tectonic evolution of the India–Eurasian Collision Zone. Eclogae Geol. Helv. 82, 717–734.
Ding, L., Kapp, P., Zhong, D., Deng, W., 2003. Cenozoic volcanism in Tibet: evidence for a transition from oceanic to continental subduction. J. Petrology 44, 1833–1865.
Ding, L., Kapp, P., Wan, X.Q., 2005. Paleocene–Eocene record of ophiolite obduction and initial India–Asia collision, south central Tibet. Tectonics 24 (TC3001), 1–18.
Ding, L., Kapp, P., Yue, Y., Lai, Q., 2007. Postcollisional calc-alkaline lavas and xenoliths from the southern Qiangtang terrane, central Tibet. Earth Planet. Sci. Lett. 254, 28–38.
Dong, G., Mo, G., Zhao, Z., Wang, L., Zhou, S., 2002. Tibet Linzhou Linzizong volcanic basin research achievements. Earth Sci. Front. 9, 153 (in Chinese).
Dong, G., Mo, X., Zhao, Z., Wang, L., Zhou, S., 2005. A new understanding of the stratigraphic successions of the Linzizong volcanics in the Linzhou Basin, northern Lhasa, Tibet, China. Geol. Bull. China 24, 549–557 (in Chinese).
Dunlop, D.J., 1995. Magnetism in rocks. J. Geophys. Res. 100, 2161–2174.
England, P., Searle, M., 1986. The Cretaceous–Tertiary deformation of the Lhasa block and its implications for crustal thickening in Tibet. Tectonics 5, 1–14.
Fielding, E., Isacks, B., Barazangi, M., Duncan, C., 1994. How flat is Tibet? Geology 22, 163–167.
Fisher, R.A., 1953. Dispersion on a sphere. Proc. R. Soc. London, Ser. A 217, 295–305.
Geological Survey of Tibet Autonomous Region (GSTAR), 2002. Regional geological survey of Shigatse, People's Republic of China, scale 1: 250, 000. Geol. Publ. House, Beijing.
Hu, X., Ma, R., Tao, X., Liu, D., 2007. Lithogeochemical characteristics and tectonic setting of volcanic rocks of Dianzhong formation in the Coqen area, Tibet, China. Sci. Techn. Edition, 34. J. Chengdu University Techn. pp. 15–22 (in Chinese).
Huang, G., Li, Zh., Qiu, R., Cai, Zh., 2004. Geologic and geochemical charateristics of volcanic rocks in Shiduo, western Gangdise, Tibet. Geosci. 18, 511–517 (in Chinese).
Huang, B.C., Piper, J.D.A., Wang, Y.C., He, H.Y., Zhu, R.X., 2005a. Paleomagnetic and geochronological constraints on the post-collisional northward convergence of the southwest Tian Shan, NW China. Tectonophysics 409 (1–4), 107–124.
Huang, Y.C., Yang, D.M., Zheng, C.Q., He, Z.H., Dai, L.N., Li, J.G., Zhang, Y.Y., 2005b. The geochemical characteristics of the Pana volcanic rocks of the Linzizong Group in the Zhaxue area, Linzhou County, Tibet and its geological implication. Earth Sci. Edition, 35. J. Jilin University, pp. 576–580 (in Chinese).
Huang, B.C., Piper, J.D.A., He, H.Y., Zhang, C.X., Zhu, R.X., 2006. Paleomagnetic and geochronological study of the Halaqiaola basalts, southern margin of the Altai Mountains, northern Xinjiang: constraints on neotectonic convergent patterns north of Tibet. J. Geophys. Res. 111, B01101. doi:10.1029/2005JB003890.
Jaeger, J.J., Adloff, C., Doubinger, J., Pons, D., Vozenin-Serra, C., Wang, N.W., 1982. The contribution of fossils to the paleogeography of the Lhasa block (Tibet). EOS 63, 1093.
Jaeger, J.J., Courtillot, V., Tapponnier, P., 1989. Paleontological view of the ages of the Deccan Traps, the Cretaceous/Tertiary boundary, and the India–Asia collision. Geology 17, 316–319.
Ji, Z.S., Yang, X.D., Zang, W.S., Yao, J.X., Wu, G.C., 2006. Advance of geochronological dating of Shexing formation in the Linzhou basin, Lhasa area and its significance. Acta Palaeontol. Sin. 45, 277–282 (in Chinese).
Johnson, M.R.W., 2002. Shortening budgets and the role of continental subduction during the India–Asian collision. Earth-Sci. Rev. 59, 101–123.
Ke, Z.H., 1990. Some Cretaceous new bivalve fossils of central Tibet. Sci. Techn. Edition, 17. J. Chengdu University Techn., pp. 31–36 (in Chinese).
Kind, R.E.A., 2002. Seismic images of crust and upper mantle beneath Tibet: evidence for Eurasian plate subduction. Science 298, 1219–1221.
Kirschvink, J.L., 1980. The least-square line and plane and the analysis of paleomagnetic data. Geophys. J. R. astr. Soc. 62, 699–718.
Klootwijk, C.T., Peirce, J.W., 1979. India's and Australia's pole path since the late Mesozoic and the India–Asia collision. Nature 282, 605–607.
Klootwijk, C.T., Gee, J.S., Peirce, J.W., Smith, G.M., McFadden, P.L., 1992. An early India–Asia contact: paleomagnetic constraints from Ninetyeast Ridge, ODP Leg 121. Geology 20, 395–398.
Klootwijk, C.T., Conaghan, P.J., Nazirullah, R., De Jong, K.A., 1994. Further paleomagnetic data from Chitral (Eastern Hindukush): evidence for an early India–Asia contact. Tectonophysics 237, 1–25.
Le Pichon, X., Fournier, M., Jolivet, J., 1992. Kinematics, topography, shortening and extrusion in the India –Asia collision. Tectonics 11, 1085–1098.
Lee, H.Y., Chung, S.L., Wang, Y.B., Zhu, D.C., Yang, J.H., Song, B., Liu, D.Y., Wu, F.Y., 2007. Age, petrogenesis and geological significance of the Linzizhong volcanic successions in the Linzhou Basin, southern Tibet: evidence from zircon U–Pb dates and Hf isotopes. Acta Petrol. Sin. 23, 493–500 (in Chinese).
Liu, H., 1993. Classification and age attribution of the Linzizong volcanic series in the Lhasa area of Tibet. Tibetan Geol. 10 (2), 59–68 (in Chinese).
Lu, B., Li, Y.T., Liu, Z., Lei, Z.Y., Xu, K.Q., 2000. Formation and classification of the basins in the Qinghai–Tibetan Plateau. Acta Petrol. Sin. 21, 21–26 (in Chinese).
Mattauer, M., Matte, P., Olivet, J.L., 1999. A 3D model of the India–Asia collision at plate scale. Geodynamics 328, 499–508.
Matte, P., Mattauer, M., Olivet, J.M., Griot, D.A., 1997. Continental subductions beneath Tibet and the Himalayan orogeny: a review. Terra Nov. 9, 264–270.
McElhinny, M.W., 1964. Statistical significance of the fold test in paleomagnetism. Geophys. J. Int. 8, 338–340.
McFadden, P.L., 1990. A new fold test for paleomagnetic studies. Geophys. J. Int. 103, 163–169.
McFadden, P.L., McElhinny, M.W., 1988. The combined analysis of remagnetization circles and direct observations in paleomagnetism. Earth Planet. Sci. Lett. 87, 161–172.
Mo, X.X., Zhao, Z.D., Deng, J.F., Dong, G.C., Zhou, S., Guo, T.Y., Zhang, S.Q., Wang, L.L., 2003. Response of volcanism to the India–Asia collision. Earth Sci. Front. 10, 135–148 (in Chinese).
Mo, X.X., Zhao, Z.D., Depaolo, D.J., Zhou, S., Dong, G.C., 2006. Three types of collisional and post-collisional magmatism in the Lhasa block, Tibet and implications for Indian intra-continental subduction and mineralization: evidence from Sr–Nd isotopes. Acta Petrol. Sin. 22, 795–803 (in Chinese).
Mo, X.X., Niu, Y.L., Dong, G.C., Zhao, Z.D., Hou, Z.Q., Su, Z., Ke, S., 2008. Contribution of syncollisional felsic magmatism to continental crust growth: a case study of the Paleogene Linzizong volcanic succession in southern Tibet. Chem. Geol. 250, 49–67.
Molnar, P., Tapponnier, P., 1975. Cenozoic tectonics of Asia: effects of a continental collision. Science 189, 419–426.
Molnar, P., England, P., Martinod, J., 1993. Mantle dynamics, the uplift of the Tibetan plateau, and the Indian monsoon. Rev. Geophys. 31, 357–396.
Owens, T.J., Zandt, G., 1997. Implications of crustal property variations for models of Tibetan plateau evolution. Nature 387, 37–43.
Pan, G., Ding, J., et al., 2005. The Qinghai–Tibet Plateau and its Adjacent Area Map 1: 1,500,000. Chengdu Map Publishing House, Chengdu, China.
Patriat, P., Achache, J., 1984. India–Eurasia collision chronology has implications for crustal shortening and driving mechanism of plates. Nature 311, 615–621.
Patzelt, A., Li, H., Wang, J., Appel, E., 1996. Paleomagnetism of Cretaceous to Tertiary sediments from southern Tibet: evidence for the extent of the northern margin of India prior to the collision with Eurasia. Tectonophysics 259, 259–284.
Powell, C.M., Conaghan, P.J., 1973. Plate tectonics and the Himalyas. Earth Planet. Sci. Lett. 20, 1–12.
Prasad, G.V.R., Rage, J.C., 1991. A discoglossid frog in the latest Cretaceous (Maastrichtian) of India. Further evidence for a terrestrial route between India and Laurasia in the latest Cretacous. C. R. Acad. Sci. 313, 272–278.
Rage, J.C., 2003. Relationships of the Malagasy fauna during the late Cretaceous: northern or southern routes ? Acta Paleontol. Pol. 48, 661–662.
Rage, J.C., Cappetta, H., Hartenberger, J.L., Jaeger, J.J., Sudre, J., Vlaney-Liaud, M., 1995. Collision age. Nature 375, 286.
Raymo, M.E., Ruddiman, W.F., 1992. Tectonic forcing of late Cenozoic climate. Nature 359, 117–122.
Schettino, A., Scotese, C.R., 2005. Apparent polar wander paths for the major continents (200 Ma to the present day): a paleomagnetic reference frame for global plate tectonic reconstructions. Geophys. J. Int. 163, 727–759.
Song, Q., 1999. Geochemical features of the volcanic rocks of Linzizong Group in Coqen basin. J. Geomechanics 5, 65–70 (in Chinese).
Tapponnier, P., Peltzer, G., LeDain, A.Y., Armijo, R., Cobbold, P., 1982. Propagating extrusion tectonics in Asia: new insights from simple experiments with plasticine. Geology 10, 611–616.
Tauxe, L., Kent, D., 2004. A simplified statistical model for the geomagnetic field and the detection of shallow bias in paleomagnetic inclinations: was the ancient magnetic field dipolar? In: Channell, J.E.T., Ken, D.V., Lowrie, W., Meert, J.G. (Eds.), Timescales of the Paleomagnetic Field, Geophysical Monograph Series, 145. American Geophysical Union, pp. 101–115.
Team of Regional Geological Survey of the Bureau of Geology and Mineral Resources of Tibet Autonomous Region (TRGST), 1990. Regional Geological map of Tibet, scale 1: 500, 000. Geol. Publ. House, Beijing.
Team of Regional Geological Survey of the Bureau of Geology and Mineral Resources of Tibet Autonomous Region (TRGST), 1991. Regional Geological map of Tibet, Lhasa, scale 1: 200,000. Geol. Publ. House, Beijing.
Tong, Y., Yang, Z., Zheng, L., 2008. Early Paleocene paleomagnetic results from southern Tibet, and tectonic implications. Int. Geol. Rev. 50, 516–562.
Torsvik, T.H., Muller, R.D., Van der Voo, R., Steinberger, B., Gaina, C., 2008. Global plate motion frames: toward a unified model. Rev. Geophys. 46 (RG3004), 1–44.
Treloar, P.J., Coward, M.P., 1991. Indian plate motion and shape—constraints on the geometry of the Himalayan Orogen. Tectonophysics 191, 189–198.

Veevers, J.J., Powell, C.M., Johnson, B.D., 1975. Greater India's place in Gondwanaland and in Asia. Earth Planet. Sci. Lett. 27, 383–387.
Wang, S.E., Liu, G., Wang, N., Yao, J., 1988. Lhasa area Mesozoic research. Professional Papers on Stratigraphy and Paleontology. Beijing, P.R. China, 20. (in Chinese).
Watson, G.S., Enkin, R.J., 1993. The fold test in paleomagnetism as a parameter estimation problem. Geophys. Res. Lett. 20, 2135–2137.
Westphal, M., Pozzi, J., Zhou, Y.X., Xing, L.S., Chen, X.Y., 1984. New evidences of paleomagnetism from Tibet, with special reference to the collision of the India with Eurasia. Sino-French Cooperative Investigation in Himalayas, pp. 17–23 (in Chinese).
Wu, X.L., Feng, Y., Huang, J.P., 2005. Geochemical characteristics of Nianbo formation at Coqen County, Tibet and its geotectonic significance. Natural Sci. Edition, 28. J. Donghua University Techn. pp. 5–11 (in Chinese).
Xu, Z., Yang, J., Li, H., Zhang, J., Zeng, J., 2006. The Qinghai–Tibet plateau and continental dynamics: a review on terrain tectonics, collisional orogenesis, and processes and mechanisms for the rise of the plateau. Geol. in China 33, 221–238 (in Chinese).
Yang, Z., Besse, J., 1993. Paleomagnetic study of Permian and Mesozoic sedimentary rocks from Northern Thailand supports the extrusion model for Indochina. Earth Planet. Sci. Lett. 117, 525–552.
Yin, A., Harrison, T.M., 2000. Geologic evolution of the Himalayan–Tibetan orogen. Ann. Rev. Earth Plant. Sci. 28, 211–280.
Zhang, K., Wang, G., Chen, F., Xu, Y., Luo, M., Xiang, S., Kou, X., Zhao, L., 2007. Coupling between the Uplift of Qinghai–Tibet Plateau and distribution of basins of Paleogene–Neogene. Earth Sci. (J. China Univ. Geosci.) 32, 583–597 (in Chinese).
Zhao, W., Nelson, K.D., Che, J., Quo, J., Lu, D., Wu, C., Liu, X., 1993. Deep seismic reflection evidence for continental underthrusting beneath southern Tibet. Nature 366, 557–559.
Zhao, W., Mechie, J., Brown, L.D., Guo, J., Haines, S., Hearn, T., Klemperer, S.L., Ma, Y.S., Meissner, R., Nelson, K.D., Ni, J.F., Pananont, P., Rapine, R., Ross, A., Saul, J., 2001. Crustal structure of central Tibet as derived from project INDEPTH wide-angle seismic data. Geophys. J. Int. 145, 486–498.
Zhou, Y.X., Lu, L.Z., Chen, X.Y., Yuan, X.G., 1990. The paleomagnetic study of the Tibetan Plateau and preliminary discussion on its tectonic evolution. In: Yuan, X.C., Zhou, Y.X., Li, L. (Eds.), Tectonic Evolution of the Lithosphere of the Himalayas—Paleomagnetic and Magnetotelluric Researches in Xizang (Tibet). Geological Memoirs, 7. Geol. Publ. House, Beijing, pp. 1–119 (in Chinese).
Zhou, S., Fang, N., Dong, G., Zhao, Z., Liu, X., 2001. Argon dating on the volcanic rocks of the Linzizong Group, Tibet. Bull. Min. Petr. Geoch. 20, 317–319 (in Chinese).
Zhou, S., Mo, X.X., Dong, G.C., Zhao, Z.D., Qiu, R.Z., Guo, T.Y., Wang, L.L., 2004. Ar-40/Ar-39 geochronology of Cenozoic Linzizong volcanic rocks from Linzhou Basin, Tibet, China, and their geological implications. Chin. Sci. Bull. 49, 1970–1979.
Zhu, Z., Teng, J., 1984. The Indian plate moving north and sub-block collision with the Eurasian plate, paleomagnetic evidence after the disintegration of Gondwanaland. Sino-French Cooperative Investigation in Himalayas, pp. 17–23 (in Chinese).
Zhu, Z., Zhu, X., Zhang, Y., 1981. Paleomagnetic observation in Xizang (Tibet) and continental drift. Acta Geophys. Sin. 24 (1), 40–49 (in Chinese).
Zhu, D., Pan, G., Mo, X., Duan, L., Liao, Z., 2004. The age of collision between India and Eurasia. Adv. Earth Sci. 19, 564–571 (in Chinese).
Zijderveld, J.D.A., 1967. A.C. demagnetization of rocks: analysis of results. In: Collinson, D.W., Creer, K.M., Runcorn, S.K. (Eds.), Methods on Paleomagnetism. Elsevier, Amsterdam, pp. 254–286.